MOLECULAR DETERMINANTS OF PHOTORECEPTOR PRESYNAPTIC TERMINAL MORPHOLOGY

A Dissertation

by

DUSTIN THAD WHITAKER

Submitted to the Office of Graduate and Professional Studies of
Texas A&M University
in partial fulfillment of the requirements for the degree of

DOCTOR OF PHILOSOPHY

Chair of Committee,	Michael Smotherman
Committee Members,	Gladys Ko
	Bruce Riley
	C. Jane Welsh
Interdisciplinary Faculty Chair,	Michael Smotherman

May 2018

Major Subject: Neuroscience

ABSTRACT

Rod and cone photoreceptors are light-receptive cells in the visual system that convert photons into an electrochemical signal to be processed through the retina and transmitted into the brain. From the first visual synapse, from photoreceptor to interneurons, rod spherules and cone pedicles diverge in morphology and connectivity patterns. It is known that the transcription factor Nrl is sufficient to drive the cone-to-rod cell fate conversion and morphological change. To dissect the source of the spherule versus pedicle differences, we performed a directed RNAi screen using *in vivo* electroporation to knock down a select portion of the Nrl regulome to identify genes associated with morphological features.

We systematically characterized four distinct features of rod spherules and S-cone pedicles: spherule width, terminal position in the outer plexiform layer, ribbon number, and presence or absence of telodendrites. Using previously published next-generation sequencing data of the transcriptome of developing rod and cone-like photoreceptors as well as key transcription factor binding profiles, we defined a set of genes potentially associated with restricting spherule morphology from that of the default pedicle state. By knocking down genes individually, we were able to dissect the effects each gene has to restrict spherules. Our screen identified twenty-seven genes that control one or two independent features of rod photoreceptor spherule morphology, terminal width or outer plexiform layer position. Many of these were confirmed either through rescue experiments or examination of loss of function mouse strains.

Lastly, we generated a protein interaction network to connect the seemingly random sets of genes that controlled spherule morphology. Clustering of genes in this network did not show enrichment of our positive screen targets into communities. When we created shortest network pathways between all pairs of positive targets, we discovered that there was an enrichment of pathways that utilized Ncoa2, and this gene has a direct path to Nrl. We hypothesize that we have discovered a more directly involved gene regulatory network associated with the restriction of rod photoreceptor spherules. This knowledge should help in blinding disease treatment strategies to improve proper integration into the native retinal circuitry after loss of photoreceptors.

DEDICATION

To the animals sacrificed now to alleviate human suffering in the future…

ACKNOWLEDGEMENTS

Too many thanks are in order to name all of the people that have provided guidance, support, or a much-needed drink along the way, but I must specifically name a few that were essential.

I would like to first thank my mentor, Dr. Anand Swaroop, for providing me with a new lab home in the middle of my graduate degree and allowing me to perform my thesis work in his laboratory. The independence, financial support, and macro management guidance provided has allowed me to become a more self-sufficient problem solver and scientist and ready for any future challenges in my career.

I would like to thank my full thesis committee, Drs. Smotherman, Ko, Riley, and Welsh, for their assistance and support in all steps of completing the doctorate, especially with the additional hurdles caused by performing my thesis at another institute they helped me overcome.

Finally, my family and friends have provided so much support along the way. There were many days when the light at the end of the tunnel seemed too distant that they reminded me of my goals and kept me on track. I have also had the pleasure of working alongside many friends who, through discussions of projects over coffee or beer, have provided advice and suggestions that have vastly improved the quality of my work.

CONTRIBUTORS AND FUNDING SOURCES

This work was performed in the laboratory of Professor Anand Swaroop at the National Eye Institute, National Institutes of Health, Bethesda, Maryland. This work was supervised by a dissertation committee consisting of Professor Michael Smotherman, committee chair, and Professor Bruce Riley of the Department of Biology and Professors Gladys Ko and C. Jane Welsh of the Department of Veterinary Integrative Biosciences.

Transmission electron microscopy image of rod spherules and cone pedicle imaged by Dr. Jessica Gumerson at the National Eye Institute and graciously gifted for this work. The RNA-sequencing data analyzed for Chapter II, Figures 7 and 8 was provided by Mr. Matthew Brooks at the National Eye Institute as a re-analysis of previously published work (Kim et al., 2016b); filtering and selection of genes was performed independently by the student. Adeno-associated virus (AAV) packaged guide RNAs for CRISPR/Cas9-mediated loss of function was designed by Dr. Wenhan (John) Yu and packaged by Ms. Suja Hiriyanna. The network analysis performed in Chapter II, Figures 15 and 16, was conducted by Dr. Anupam Mondal of the National Eye Institute. Interpretation of the data was a collaborative effort between Dr. Mondal and myself.

All other work conducted for the dissertation was completed by the student independently.

First-year and summer graduate study were supported by a fellowship from the Texas A&M Institute for Neuroscience. Dissertation research was supported through the Intramural Research Training Award at the National Eye Institute intramural program, NIH.

NOMENCLATURE

AAV	Adeno-associated virus
AMD	Age-related macular degeneration
DR	Diabetic retinopathy
GCL	Ganglion cell layer
GRN	Gene regulatory network
INL	Inner nuclear layer
IPL	Inner plexiform layer
iPSC	Induced pluripotent stem cell
IS	Inner segment
ONL	Outer nuclear layer
OPL	Outer plexiform layer
OS	Outer segment
RDD	Retinal degenerative disease
RP	Retinitis pigmentosa
RPE	Retinal pigment epithelium

TABLE OF CONTENTS

LIST OF FIGURES

LIST OF TABLES

CHAPTER I

INTRODUCTION: PHOTORECEPTOR SYNAPTIC TERMINAL DEVELOPMENT AND FUNCTION

Introduction

The vertebrate retina is an ordered neural circuit in the eye responsible for the recognition, processing, and transmission of light signal from the external environment to the brain. Five major classes of neurons (photoreceptor, bipolar, horizontal, amacrine, and ganglion) and one glial cell (Müller) are arranged into three distinct lamina of cell bodies with connective, cell-free layers between the nuclear layers (Figure 1) (Masland, 2001a, b). Light photons enter the anterior eye and are detected by rod and cone photoreceptors and are converted to an electrochemical signal. The signal undergoes multiple levels of processing and refinement through the outer and inner plexiform layer (OPL and IPL, respectively) as it passes from photoreceptors to interneurons to ganglion cells, which direct transmit these signals to the brain.

Photoreceptors detect light through photosensitive opsins in the outer segments of the cells; this signal is amplified through the phototransduction cascade to cause the closure of calcium channels and hyperpolarization of the membrane. Due to the dynamic temporal properties and requirement of sustained signaling for sensing light, vertebrate photoreceptors have evolved, among other things, to use a special synaptic active zone feature, termed the synaptic ribbon, to provide constant neurotransmitter release that can be adjusted in graded increments for most of the dynamic range of light signals (Schmitz

et al., 2000; Lamb et al., 2007). Photoreceptors connect directly with two classes of interneurons (horizontal and bipolar) in the OPL to form the first visual synapse. The presynaptic terminals of rods and cones, spherules and pedicles, respectively (Figure 2), have some distinct properties making each type of terminal unique. This chapter focuses on four key morphological features that are important for photoreceptor function: the connectivity patterns in the OPL, ribbon structure and transmission, gap junctions for alternative cell-cell communication, and size and structure of synaptic terminals.

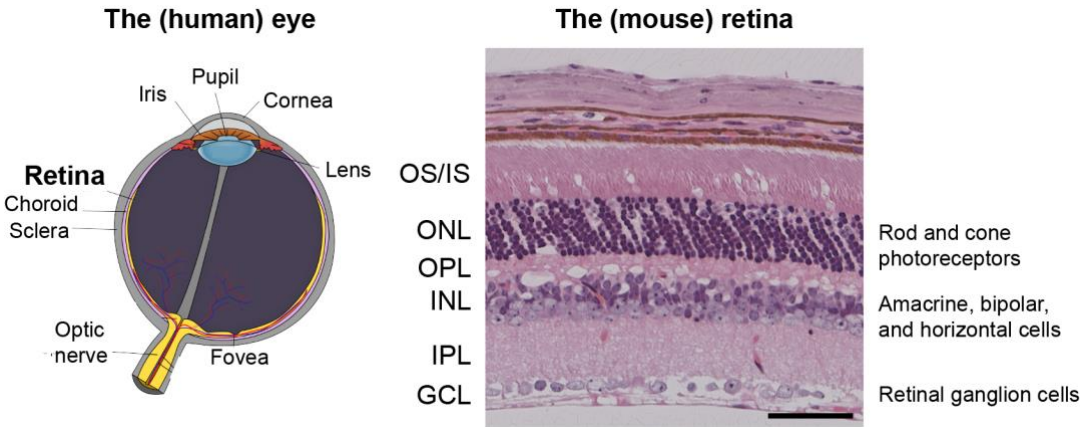

Figure 1. The eye and retina. (left) A schematic representation of the human eye[1]. The retina (name bolded) is a thin tissue that lines the posterior portion of the eye. One major difference between human and mouse retinas is that humans contain a fovea (rod-free portion of the retina) whereas mice do not contain this feature. (right) Histological section of the mouse retina. Lamination of distinct layers is easily seen. Layer abbreviations indicated on left and cell types within each nuclear layer on the right. OS/IS: outer/inner segments; ONL: outer nuclear layer; OPL: outer plexiform layer; INL: inner nuclear layer; IPL: inner plexiform layer; GCL: ganglion cell layer

[1] Modified (enlarged labels) from: Soerfm (Own work) [CC BY-SA 3.0 (https://creativecommons.org/licenses/by-sa/3.0)], via Wikimedia Commons

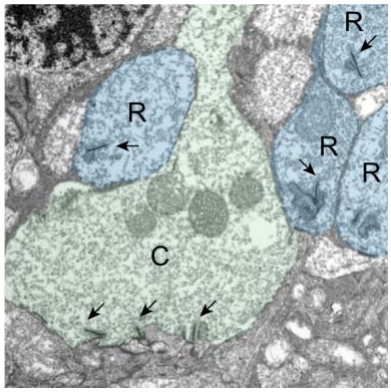

Figure 2. Spherules and pedicle. Transmission electron microscopy image of the retinal outer plexiform layer (OPL). Three of the four features that we discuss in this chapter can be seen in this image: (1) Rod spherules ("R") are smaller than cone pedicles ("C"). (2) Each spherule only has a single ribbon; three can be seen in this pedicle. And (3) pedicles penetrate deeper into the OPL (photoreceptor cell bodies out of frame on the top). Arrows indicate synaptic ribbon.

The central nervous system (CNS) is a complex network comprised of billions of neurons and trillions of connections (Pakkenberg et al., 2003; Azevedo et al., 2009). In many cases, two interacting neurons within the CNS can be separated by quite a distance, making investigations of circuit assembly and function difficult. The easily accessible retina provides an accessible model in which to study circuitry due to its highly stereotypic design, increasingly well-defined developmental programs, and has a distinct starting point (photon signal reaching photoreceptors). Similar mechanisms occur in the invertebrate visual system (Sanes and Zipursky, 2010). While the majority of circuity analysis in the retina has been performed in the IPL, we believe that the OPL actually provides a more simple and restricted set of connections that could be used to model some features of almost any other neural network. The rod photoreceptor circuitry alone, for

example, can illustrate many network features such as axon guidance and synaptogenesis (Sanes and Yamagata, 2009), signaling and feedback (Demb and Singer, 2015), convergence/divergence (Wassle, 2004), and study and treatment of neurodegenerative diseases (Stone, 2009).

Loss of photoreceptors results in the majority of retinal degenerative diseases causing irreversible blindness (Veleri et al., 2015). The genes associated with photoreceptor loss cover a wide spectrum of cellular localizations and functions (see RetNet for comprehensive database of retinal diseases and associated genes: https://sph.uth.edu/retnet), and those found at the synaptic terminals are no exception. A few known causes of synaptic terminal-influenced retinal dysfunctions or degenerations are reviewed here, and the last section discusses how many likely treatments for blinding diseases can utilize the knowledge found of the photoreceptor synaptic morphology and circuit development.

The first visual synapse in the OPL

We begin our discussion of rod and cone terminals by placing them into their natural environment within the OPL. This small, cell-free layer houses the synaptic terminals of photoreceptors, rod spherules and cone pedicles, with dendrites of bipolar cells and both axons and dendrites of horizontal cells. Photoreceptor-to-interneuron connections within the OPL are highly stereotyped, making the OPL an ideal region for investigation into the mechanisms regulating neurite projections, guidance cues, and remodeling. The OPL can be divided roughly into two halves based on which cells

connect: (1) the region closest to the photoreceptor cell bodies contains rod spherules connecting to a single rod bipolar and horizontal cell axons; (2) the region closer to interneuron bodies connects pedicles to many cone bipolar cell types and the dendrites of horizontal cells (Kolb, 1970, 1977; Euler et al., 2014). Rods and cones also make additional connections that do not follow the standard pathways. For example, rods employ two alternative pathways to transmit signal through the retina: (1) a gap junction between rod and cone terminals sends signals through depolarizing (ON-center) cone bipolar cells; (2) rods connect directly to hyperpolarizing (OFF-center) cone bipolar cells through an electrical gap junction (Deans et al., 2002; Volgyi et al., 2004). Signal transfer from photoreceptors to bipolar cells does not proceed through a 1:1 connectivity ratio (except in the midget pathways in the fovea, discussed briefly below); both convergent and divergent signaling mechanisms are employed in the OPL, though at different scales between rods and cones (Wassle, 2004). Convergence of multiple pre-synaptic terminals onto a single post-synaptic dendrite improves sensitivity of signal transfer, though at a cost of visual acuity loss. Rods show a convergence of 45 – 55 rods synapsing on a single rod bipolar (Anastassov et al., 2017), much higher than previously thought (Tsukamoto and Omi, 2013); in cone photoreceptors, approximately 4 – 6 pedicles will synapse onto each cone bipolar (Cohen and Sterling, 1990). In the primate/human fovea, visual acuity needs to be greatest, so cones have evolved the minimum convergence rates, 1 cone:1 bipolar, to maximize acuity. Divergence increases signal transmitted through the system by transmission to multiple downstream post-synaptic cells. Spherules connect to two rod bipolar cells; divergence in rods could also be described of the alternative pathways

(above). In cones, each pedicle will connect only once to each class of bipolar cell but makes synapses onto each of their different downstream bipolar classes (Cohen and Sterling, 1990). Again, divergence is kept low in the fovea with each cone connecting to only 2 bipolar cells (one ON and one OFF).

The developmental timeline of photoreceptor axon and interneuron dendrite formation has been charted. Photoreceptor synaptic connections are all made during early postnatal development (Olney, 1968; Blanks et al., 1974; Rich et al., 1997). The majority of rod spherule connection to both interneurons happens within the first postnatal week and are defined before eye opening. Cones synapse with horizontal cells almost immediately after birth but take almost two weeks to connect with bipolar cells (Rich et al., 1997). Bipolar cell connections are formed later than horizontal connections due to the finding that bipolar cell neurites (dendritic and axonic projections) originally span the entire retina, and only during postnatal development do dendrites retract to laminate at the OPL with rods and cones (Morgan et al., 2006). But each cone-bipolar cell synapse stabilizes at different time points in development, depending on the type of bipolar cell; this indicates some intrinsic bipolar cell mechanisms to stabilize synapses (Dunn and Wong, 2012). Formation and stabilization of photoreceptor circuits could rely on molecular and/or signaling mechanisms. In fact, both mechanisms in combination form photoreceptor synapses. Some molecules required for synaptogenesis and/or stabilization of photoreceptors to bipolar cells have been identified (Sato et al., 2008; Omori et al., 2012), as well as others that are required for *specific* cell-to-cell recognition, including: Ngl-2 for rod to horizontal cell axons (Soto et al., 2013) and Elfn1 for rod to rod bipolar

connections (Cao et al., 2015). Loss of any of these molecules shows complete lack of synaptic transmission between neurons. In addition, neurotransmission regulation of neurite formation and synaptogenesis is generally true in the CNS (Wong and Ghosh, 2002). Cones seem more impaired by lack of sensory experiences than rods (Dunn et al., 2013), with altered synapses with some cone bipolar cell types; rods may use alternative methods for forming the appropriate connections as their synapses are already stabilized before eye opening.

Ribbon synapses allow tonic, graded neurotransmission

Some sensory systems (including vision, hearing, and balance) require their neurons to convert incoming environmental to electrochemical synaptic signals over a wide range of intensities and time scales. These cells have evolved a specialized organelle to allow for sustained release of neurotransmitter at the synaptic active zone, the ribbon. The ribbon was originally found in photoreceptors (De Robertis and Franchi, 1956), but is also located in other sensory neurons in the CNS. This structure is essential to maintaining proper vesicular transport and exocytosis (Snellman et al., 2011; Mehta et al., 2013). A similar structure found in *Drosophila* is the T-bar (Prokop and Meinertzhagen, 2006), but the evolutionary origins are probably distinct. Ribbons are easily identifiable in electron microscopy images of photoreceptors by their long, electrodense (dark) structures that extend from the inner membrane into the presynaptic cell with many vesicles coating both sides of the ribbon. The three-dimensional structure of the rod photoreceptor ribbon is actually a curved, sheet-like structure that curves around the

horizontal and bipolar cell invaginations (Rao-Mirotznik et al., 1995). Not all ribbons are equal, and rod and cone photoreceptors have different ribbon structural dimensions (reviewed in (Baden et al., 2013)), with rods having a single, larger ribbon and cones containing multiple smaller, shorter ribbons. Larger rod ribbons contain an associated larger number of vesicles than the smaller cone ribbons (rod: 600-700 with 100-130 docked; cones: 100-300 with 20-60 docked). This large number of vesicles docked to ribbons is necessary for the continuous exocytosis of neurotransmitter found in photoreceptors (below).

Many of the protein components found in the cytomatrix of the active zone in conventional synapses (Sudhof, 2012) also help make up ribbon synapses, potentially with the sensory synapse evolving later and repurposing many features. One component of the ribbon – Ribeye – is excusive to this structure and essential for its formation (Schmitz et al., 2000; Magupalli et al., 2008; Lv et al., 2016; Maxeiner et al., 2016). The other active zone proteins are divided into two domains at ribbon synapses: associated directly with the ribbon and located at its base by the membrane (tom Dieck et al., 2005). The former group consists of Rim1, Kif3a, CtBP1, Piccolo – now thought to be a Piccolo-truncated variant Piccolino, and Unc119 (Wang et al., 1997; Muresan et al., 1999; tom Dieck et al., 2005; Alpadi et al., 2008; Regus-Leidig et al., 2013). The latter group, involved in anchoring of the ribbon as well as assisting in exocytosis, is composed of Bassoon, Rim2, Munc13-2, Cast1, CABP4, and L-type calcium channels (CaV1.4) (Dick et al., 2003; Haeseleer et al., 2004; tom Dieck et al., 2005; Cooper et al., 2012).

Ribbons are not constructed directly from the synapse active zone. Instead, spherical, electrodense ribbon precursors are detected as early as P2-4 in the soma and axon of photoreceptors; these "precursor spheres" contain Ribeye, Bassoon, Piccolo (now likely Piccolino, see above), and vesicles that traffic down into the synaptic terminal (Regus-Leidig et al., 2009). During this period, remodeling of the ribbon occurs to first transition from spherical to planar ribbons, through a yet unknown mechanism, and second to anchor ribbons into the active zone at the terminals (Regus-Leidig et al., 2009). Loss of Bassoon demonstrated its importance to the initial formation of precursor spheres, transition from spherical to planar ribbons, and anchoring of ribbons (Dick et al., 2003; Regus-Leidig et al., 2010); precursor spheres are not present until later development (P10), and there is a complete lack of attached ribbons. Bassoon, along with Ribeye, also helps in the assembly of a large number of vesicle release sites by organizing calcium channels (Frank et al., 2010). Once part of the mature ribbon complex, ribeye turnover is relatively low (Graydon et al., 2017); Piccolino and CAST are both important for the stabilization of the mature ribbon structure, as reduction of either leads to ribbon "breaking" or being shortened, but they are not responsible to mount ribbons to the active zone like Bassoon (tom Dieck et al., 2012; Regus-Leidig et al., 2014).

As mentioned above, ribbons are found in sensory neurons requiring a graded and continuous transmission of signal. Photoreceptors undergo two types of exocytosis: transient and sustained; these allow the synapse be able to immediately respond to stimuli as well as continue responding over long time scales. Photoreceptors are continuously depolarized in their dark, resting state with calcium channels open and neurotransmitter

being released. Light, through phototransduction, hyperpolarize cells, shut calcium channels, and inhibit vesicle release. At the onset of dark conditions, rods and cones begin releasing vesicles and can transmit up to 100 vesicles per ribbon per second, but rates of release are often <1 vesicle release site per second allowing for sustained release (van Rossum and Smith, 1998; Heidelberger et al., 2005). This rate is no faster than found at amacrine or hippocampal synapses, only prolonged. Cones have faster initiation and termination of signal than rods with a more extended decay rate (Rabl et al., 2005). Complexins3/4 have been found to also decrease noise within the system by reducing spontaneous release of vesicles (Vaithianathan et al., 2015; Babai et al., 2016).

Vesicle populations at ribbon synapses correlate with those of conventional synapses (readily releasable/docked, recycling pool, and a reserve), though photoreceptors have a bias towards more vesicles in the readily releasable and recycling pools (von Gersdorff et al., 1996; Rizzoli and Betz, 2005; Datta et al., 2017). In photoreceptors, the recycling pool are those vesicles found on the ribbon itself. There are three main hypotheses (not necessarily mutually exclusive) for vesicle transfer and synaptic fusion on the ribbon: (1) an active conveyor belt to shuttle vesicles down the ribbon, (2) passive diffusion of vesicles along ribbon, and (3) compound fusion in which vesicles may merge along the ribbon to release vesicular components together. These are discussed in more detail elsewhere (Matthews and Fuchs, 2010), but based on recent evidence, we believe that the model of passive vesicle diffusion along the ribbon is the main contributor of vesicle dynamics on the ribbon (Heidelberger et al., 2002; Holt et al., 2004; Chen et al., 2013; Graydon et al., 2014). These synaptic terminals are fascinating because of their

evolutionary specialization of the ribbon organelle and its contributions to maintaining both fast and long neurotransmitter release rates.

Photoreceptor coupling by telodendrites

Telodendrites are long and thin neurite projections extending from cone pedicles to contact neighboring cone or rod photoreceptors through an electrical gap junction (Raviola and Gilula, 1973, 1975). These projections were found in all vertebrate species (Cohen, 1965; Dowling and Boycott, 1966; Raviola and Gilula, 1973, 1975; Kolb, 1977; Ohtsuka and Kawamata, 1990; Fadool, 2003; Noel and Allison, 2017). In mammals these have only been found in cones whereas in some aquatic species they are also found in rods as well (Ohtsuka and Kawamata, 1990; Fadool, 2003; Noel and Allison, 2017), but rods do still connect to one another through gap junctions in mammals (Raviola and Gilula, 1973). A systematic analysis of telodendrites in the primate retina found that each cone possessed between 4 – 10 neurites with lengths that varied based on the packing density of cones with shorter telodendrites in the central retina (0.8 ± 0.3µm) to longer in the periphery (mid: 2.3 ± 0.9µm; far: 3.9 ± 1.8µm) with some extremely long examples of up to 10µm (O'Brien et al., 2012). In addition to anatomical location of cones within the retina, the subclass of cone also affects telodendrite connectivity. The short-wavelength, "blue," cone is much more generally isolated from other cones but connects heavily to neighboring rod spherules (approximately 90%). Medium- and long-wavelength, "green" or "red," cone telodendrites connect more to other cones (70%) with the majority being homologous connections (i.e. red-to-red) due to the non-random mosaic patterning in

higher mammals (Hsu et al., 2000), but some heterologous connections occur that cause a slight reduction in color discrimination (Hornstein et al., 2004).

The major gap junction protein of the retina was found to be Connexin35 (Cx35) in the skate, and the homologous protein in mammals as Cx36 (O'Brien et al., 1996; Sohl et al., 1998). A Cx36 reporter line found expression of the gene to be in many retinal neurons, including all photoreceptors (Deans et al., 2002), but protein localization was only detectable at the telodendrite tips in cones (Lee et al., 2003; Feigenspan et al., 2004; Zhang and Wu, 2004). The Connexin, or other gap junction protein, located in the spherule is still debated (Deans et al., 2002; Lee et al., 2003; Feigenspan et al., 2004; Bolte et al., 2016; Kim et al., 2016b). These gap junctions are dynamically regulated by circadian rhythms with more opening during the night than the day (Ribelayga et al., 2008; Li et al., 2009a; Zhang et al., 2015) with similar effects based on lighting conditions (Li et al., 2013). Coupling during the day is controlled through phosphorylation of two internal amino acids (Serines 110 and 276) (Kothmann et al., 2007) by opposing dopamine and adenylate cyclase pathways effects on Protein Kinase A (Ouyang et al., 2005; Li et al., 2013).

The development of gap junctions between photoreceptors leads to three major improvements in the visual system that will be discussed more below: increased signal-to-noise ratios, increased dynamic range within mesopic light, and rod-cone coupling creating one alternative rod visual pathway (above) (Bloomfield and Volgyi, 2009). In the turtle retina, a stimulus from one cone could be detected in neighboring cones up to 40μm away (Baylor et al., 1971), but calculations actually predicted that, at least in the human

fovea, would have a detrimental effect on visual acuity and causing a blurring effect (DeVries et al., 2002). So, what is the purpose of such an apparatus? While these connections *do* cause a slight blurring (by 0.5 cone diameters in the fovea), this is under the optical blur of the eye. The real improvement of the system comes from the improvement of the signal-to-noise ratio in cones (approximately 77%) by minimizing the intrinsic noise coming from a single cone as its neighbors have their own noise patterns; it also increases the signal intensity comes from true visual activity (DeVries et al., 2002). Rod-to-rod coupling increases the dynamic range of scotopic light detected (Publio et al., 2009); it also helps pool rod photoreceptor signals to send through an OFF cone bipolar cell as only approximately 20% of rods contact these bipolar cells. (Tsukamoto et al., 2001). Rod-to-cone signaling through telodendrite gap junctions provides yet another alternative pathway for rod visual signaling during mesopic conditions, when rod-to-rod bipolar signaling is near saturation but cone signals are near but not over threshold, extending the working range of rod photoreceptors (Hornstein et al., 2005; Abd-El-Barr et al., 2009; O'Brien et al., 2012; Asteriti et al., 2014).

General dimensions of spherules and pedicles

Comparing photoreceptor terminals shows gross morphological size differences found between and within the two classes. Ramon y Cajal detected by using the Golgi stain that the two classes of photoreceptors possessed terminals with different volumes and area. Later electron microscopy in cat photoreceptors gave the first estimates of terminal size with a diameter of 3μm for spherules and 5-8 μm for pedicles; the axons of

photoreceptors also vary in diameter with an extremely thin rod axon (0.25µm) and a much larger cone axon (1.5µm) (Kolb, 1977), though these both are on the smaller end of the axon diameter spectrum (Perge et al., 2012). Later studies confirmed that the terminal size differentials between photoreceptors are common in other mammals (Cohen, 1965; Dowling and Boycott, 1966; Olney, 1968) and some other aquatic species (Goede and Kolb, 1994; Tarboush et al., 2012). Size distinctions are not only found between rods and cones. Cone sub-classes also often have differently size pedicles; in mammals, the default blue cone pedicles are smaller than their red/green counterparts ((Breuninger et al., 2011; O'Brien et al., 2012), D.T.W. and A.S., unpublished observations); in the only study referencing pedicle size in an aquatic species; the turtle's six photoreceptor classes (1 rod and 5 cones) have four main size distributions (Goede and Kolb, 1994). The genetic and molecular causes creating differently size terminals is still mostly unknown. In mammals, the transcription factor NRL is sufficient to drive a S-cone to rod cell fate switch (Mears et al., 2001; Oh et al., 2007), with corresponding pedicle to spherule morphology change (Strettoi et al., 2004), so it could be predicted that some yet unknown transcriptional target(s) of NRL is driving terminal size changes. Unfortunately, the functional implications of smaller versus larger terminals has not been actively tested and will remain an open question.

Synaptic dysfunction results in blinding diseases

Vision loss is considered one of the worst health conditions (Scott et al., 2016). The leading blinding diseases (and approximate incidence) are: cataracts – clouding of the

lens in the eye, glaucoma – increased eye pressure damaging the optic nerve (~13% over the age of 40) (Malihi et al., 2014), age-related macular degeneration (AMD, ~2% of the U.S. population) (Friedman et al., 2004), diabetic retinopathy (DR, ~100 million worldwide) (Lee et al., 2015), and others, including retinal degenerative diseases (RDDs) (Congdon et al., 2004). Of these, AMD, DR, and RDDs affect photoreceptor physiological function and survival. Mendelian forms of retinal dystrophy have rates of 1 in 2,000 – 3,000 (Hartong et al., 2006) with dysfunction or degeneration of photoreceptors accounting for the majority of RDDs (Hoon et al., 2014; Veleri et al., 2015).

The Online Mendelian Inheritance in Man® genetic database (OMIM®: https://www.ncbi.nlm.nih.gov/omim) contains approximately 1,500 entries of inherited diseases (either syndromic or non-syndromic) with an associated retinal dysfunction (Berger et al., 2010). Over 250 causative genes have currently been identified (RetNet: https://sph.uth.edu/retnet) with no plateau seen yet in the identification of loci associated with Mendelian retinal diseases, but the advent of next-generation sequencing technologies combined with improved diagnosis procedures improves the rates of candidate gene detection in patients (Ratnapriya and Swaroop, 2013). Causative genes in photoreceptor dysfunction are known to span across all sub-compartments of rods and cones, from the outer segments to the synaptic terminal. Mutations in three proteins associated with calcium binding or calcium channels (CaBP4 (Zeitz et al., 2006), Cacna1f (Bech-Hansen et al., 1998), and Cacna2d4 (Wycisk et al., 2006)) have been linked to multiple distinct cases of congenital stationary night blindness or cone-rod dystrophy, and mouse models, either knockout or spontaneous mutants, have shown similar effects as

patients. Other ribbon-associated (Rims1 or Tulp1) proteins are also implicated in the RDDs or loss of an electroretinogram (ERG) b-wave – indicative of photoreceptor to ON-bipolar neurotransmission (Hagstrom et al., 1998; Kelsell et al., 1998; Johnson et al., 2003). Even mutations or loss of Grm6, Lrit3 Trpm1, three proteins localized to the post-synaptic, bipolar side of the membrane and important for synapse formation, can also cause circuit dysfunction or photoreceptor loss (Barnes et al., 2002; Li et al., 2009b; van Genderen et al., 2009; Zeitz et al., 2013).

Future treatments of RDDs

Multiple approached have been put forth for treatment of blinding diseases, not only those above but all photoreceptor-related RDDs. The three main strategies include gene therapy, cell therapy, and reprogramming of glial cells into photoreceptors *in vivo*. Regardless of the approach taken, photoreceptor integration with interneurons and proper synaptic function are essential elements for visual function, and without these two features, no amount of visual detection by the cells will be communicated to the brain. Gene therapy, to correct a causative mutation or supplement gene expression, will be most effective prior to or at the earliest detection of photoreceptor degeneration. Ou and colleagues (Ou et al., 2015) demonstrated that delivery of Rs1 by adeno-associated virus (AAV) in a mouse model of the synaptic disease X-linked retinoschisis restored proper localization of key molecular components as well as visual function; a clinical trial involving this study is already recruiting (NCT02317887). Cell therapy involves the transplantation of photoreceptor precursors into a degenerated retina to replace lost

photoreceptors with donor precursors derived from a stem cell population to reintegrate into the circuit and restore visual function (Zarbin, 2016). Early reports showed promising integration and visual recovery by transplantation of precursors (MacLaren et al., 2006), but a setback for the field occurred when it was discovered that donor cells are not actually integrating but instead transferring RNA and/or protein to remaining host photoreceptors (Pearson et al., 2016). This data does not, however, negate the fact that late-stage degeneration without any remaining photoreceptors do show integration and visual improvement (Barber et al., 2013; Singh et al., 2013), making reversing blindness possible. The integration precision and efficiency of these cells will require further testing (Zarbin, 2016). *In vivo* regeneration of degenerated photoreceptors (and other cell types in the retina) through Müller cell reprogramming is a natural occurrence in some species, including zebrafish (Wan and Goldman, 2016), and neural reprogramming has recently been induced in adult mammals, though not yet for photoreceptors (Jorstad et al., 2017). This provides great promise for treatment of blinding diseases (in combination with gene therapy if the cause is genetic). Greater knowledge of the developmental programs underlying proper cell-to-cell synaptogenesis and morphogenesis will be required, though, because reprogrammed neurons, even in a naturally occurring model, do not fully recapitulate their original structures (D'Orazi et al., 2016) and timing of reprogramming influences proper connectivity (Yoshimatsu et al., 2016).

Conclusions

We have discussed the development and function of both rod and cone synaptic terminals and highlighted four features that are essential for proper connectivity and physiological functional. These data do not fully do justice to the full complexity of unique features within or between photoreceptor terminals but provide the reader with a foundation upon which other differences can be built. Study of spherules and pedicles during development and in their fully mature states is essential for future treatment of blinding diseases, and it can even provide a simplified model for other neurodegenerative diseases involving synaptic dysfunction or treatments requiring reconnection between pre- and post-synaptic neurons. Many questions remain however, but the future of photoreceptor synaptic biology is bright.

CHAPTER II

MOLECULAR DETERMINANTS OF PHOTORECEPTOR PRESYNAPTIC TERMINAL MORPHOLOGY

Overview

Light photons captured by the rod and cone photoreceptors produce distinct visual information that is transmitted through ribbon synapses with interneurons. Unique presynaptic structure of rod and cone photoreceptors, called spherule and pedicle, respectively, dictates the formation of specific neuronal circuits. We took advantage of transcriptome profiles of the developing mouse rod photoreceptors and Nrl-mediated regulatory network to identify 720 candidate genes that potentially control presynaptic terminal formation. Knockdown of 78 selected genes *in vivo* identified seven genes that increased size of rod spherules and 25 showing significantly altered position of the terminal in the synaptic layer. Reintroduction of seven cDNAs with their cognate shRNA recovered the original spherule morphology. Loss of function of four genes in the mouse retina demonstrated altered terminal width. Protein interaction network analysis revealed multiple genes and Nrl-downstream pathways that might potentially modify rod presynapse morphogenesis. Our studies provide the foundation for elucidating the architecture of first visual synaptic circuit in the mammalian retina and assist in designing photoreceptor replacement therapies for retinal degenerative diseases.

Introduction

The human central nervous system (CNS) contains almost 86 billion neurons that form over 150 trillion synapses (Pakkenberg et al., 2003; Azevedo et al., 2009). Within this complex system, each neuronal subtype possesses a highly stereotyped morphological standard, precise synaptic connections, and distinct physiological function. Even slight deviations from the norm can be detrimental and cause neuronal dysfunction or even death (van Spronsen and Hoogenraad, 2010; Siskova et al., 2014; Wijetunge et al., 2014). During CNS development, an intrinsic gene regulatory network (GRN) program controls a series of cell fate decisions, that in combination with the cell's microenvironment and extrinsic stimuli, lead to individual neuronal classes (Grocott et al., 2012; Gregory-Evans et al., 2013; Syed et al., 2017); alterations in the activity of even a single gene can shift the natural balance resulting in varying phenotypic manifestations (Lee and Pfaff, 2001; Kamachi and Kondoh, 2013). The developmental trajectory of a neuron constricts its structural features towards that of its class norms to ensure appropriate morphology and communication between neurons, but the genetic determinants needed to define a neuron's structure and circuit connections are often unclear.

The retina offers an easily tractable neural pathway to investigate intrinsic and extrinsic elements for determining cell fate and maturation of a neuron within a circuit due to its laminated structure with defined regions of synaptic connectivity, high stereotypy, and ease of access for experimental manipulation. In addition to one type of Müller glia, five major classes of neurons contribute to retinal circuitry: photoreceptors, bipolar cells, horizontal cells, amacrine cells, and ganglion cells (Figure 1A), and each class consists of

between 2 and 70 subtypes (Masland, 2012). Within the outer plexiform layer (OPL) between photoreceptor and interneuron nuclei, rod and cone photoreceptors synapse onto bipolar and horizontal cells using a specialized ribbon organelle for sustained, graded neurotransmission (De Robertis and Franchi, 1956; Dowling and Boycott, 1966; Kolb, 1970). Rod circuitry provides a model circuit because it connects to only a single class of bipolar and single horizontal cell connected to the rods; the inner retina circuitry dedicated to transmission of rod photoreceptor signal also is well defined (Strettoi et al., 1990; Strettoi et al., 1992). This allows for an easy assay of how genetic alterations during rod development affects the mature retinal circuitry (Kolb, 1970; Peichl and Gonzalez-Soriano, 1994).

The majority, if not all, rod photoreceptors originate as a short-wavelength (S-, "blue") cone (Kim et al., 2016a). The induction of the transcription factor Neural Retina Leucine zipper protein (NRL) is both necessary and sufficient to actively transition from this cone to the rod cell fate (Mears et al., 2001; Oh et al., 2007; Oh et al., 2008), and NRL induces the expression of many rod photoreceptor-specific genes (Rehemtulla et al., 1996; Mitton et al., 2000; Yadav et al., 2014) with other key transcription factors (reviewed by Swaroop et al. (2010); Brzezinski and Reh (2015)). Loss of *Nrl* in rods alters the functionality and appearance of the rods to partially resemble the default S-cone state, including a spherule, rod terminal) towards pedicle (cone) morphological transition (Mears et al., 2001; Strettoi et al., 2004). Interestingly, the rod transcriptome drastically modifies a portion of its transcriptome around the period of peak rod synaptogenesis, without a similar trend in cone-like cells (Blanks et al., 1974; Kim et al., 2016b). As

spherule morphology in maturing during this same period, it could be predicted that a shift in gene expression represents an active divergence away from the cone pedicle morphology through activation of rod-enriched and/or repression of cone-enriched gene expression. Similar predictions were validated when reduction of NRL transcriptional targets produced a cone-like cell body positioning in the outer nuclear layer (ONL) (Hao et al., 2012).

We hypothesize that a portion of the NRL gene regulatory network (GRN) restricts pedicle formation in favor of spherules, and reduction/loss of these factors will relax this constraint and show pedicle-like features. In our current study, we systematically characterized murine photoreceptor synaptic terminals, identified genes that are essential for rod spherules formation through an RNAi screen, and created a curated protein interaction network to identify pathways involved in morphogenesis. Understanding the molecular determinants defining photoreceptor synaptic morphogenesis and circuit connectivity will be necessary for future treatments for blinding diseases involving gene or cell therapy, and this study identifies genes necessary for proper rod photoreceptor circuit assembly.

Assay parameters to examine presynaptic structure

Similarities and differences in gross morphology between spherules and pedicles have been noted since the original characterization of the retina. Our current analysis looks to systematically address the differences between rod and S-cone (and cone-like) photoreceptors for our present and future molecular determinant screens. We found that

rod and cone photoreceptors diverge in four gross morphological features at their synaptic terminals (Figure 3A-3C): overall diameter of terminals, sub-lamination pattern in OPL, number of synaptic ribbons active zones, and presence of telodendrites. Spherule diameter is much smaller than either cone or cone-like pedicles (rods: 2.091±0.011µm; S-cones: 4.917±0.092µm; cone-like: 3.036±0.063µm) and do not contain the presence of telodendrite projections from the terminal body as in cones (Figure 3D). In our wild type rod and cone terminals, we see distinct lamination within the OPL with spherules synapsing close to photoreceptor cell bodies and pedicles closer to interneurons (Figure 3E; rod: 0.796±0.005 relative distance; S-cone: 0.449±0.015). Cone-like lamination is more widely distributed throughout the OPL (Figure 3E; cone-like: 0.628±0.127). The typical rod shows only a single synaptic ribbon, part of the photoreceptor active zone complex; S-cones have many more ribbons to utilize increased numbers of synaptic connections (Figure 3F; rod median: 1; S-cones: 8; cone-like: 2). For terminal width, OPL position, and ribbon number, we defined spherule parameters along two anatomical axes (dorsal/ventral and nasal/temporal) to ensure that all rod photoreceptors are the same. We found no significant deviations regardless of retinal position (Figure 4). Since there are eight layers of photoreceptors in the ONL, we checked terminal width and OPL position against cell body position within the ONL. When measuring a set of sparsely labeled cells where cell body, axon, and terminal could all be identified and quantitated together (see schematic in Figure 5), we could check how photoreceptor position in the ONL affected either variable. Again, there was no relationship between the ONL position and either phenotype or between the two phenotypes. (Figure 6). All of these data (Table1) provide

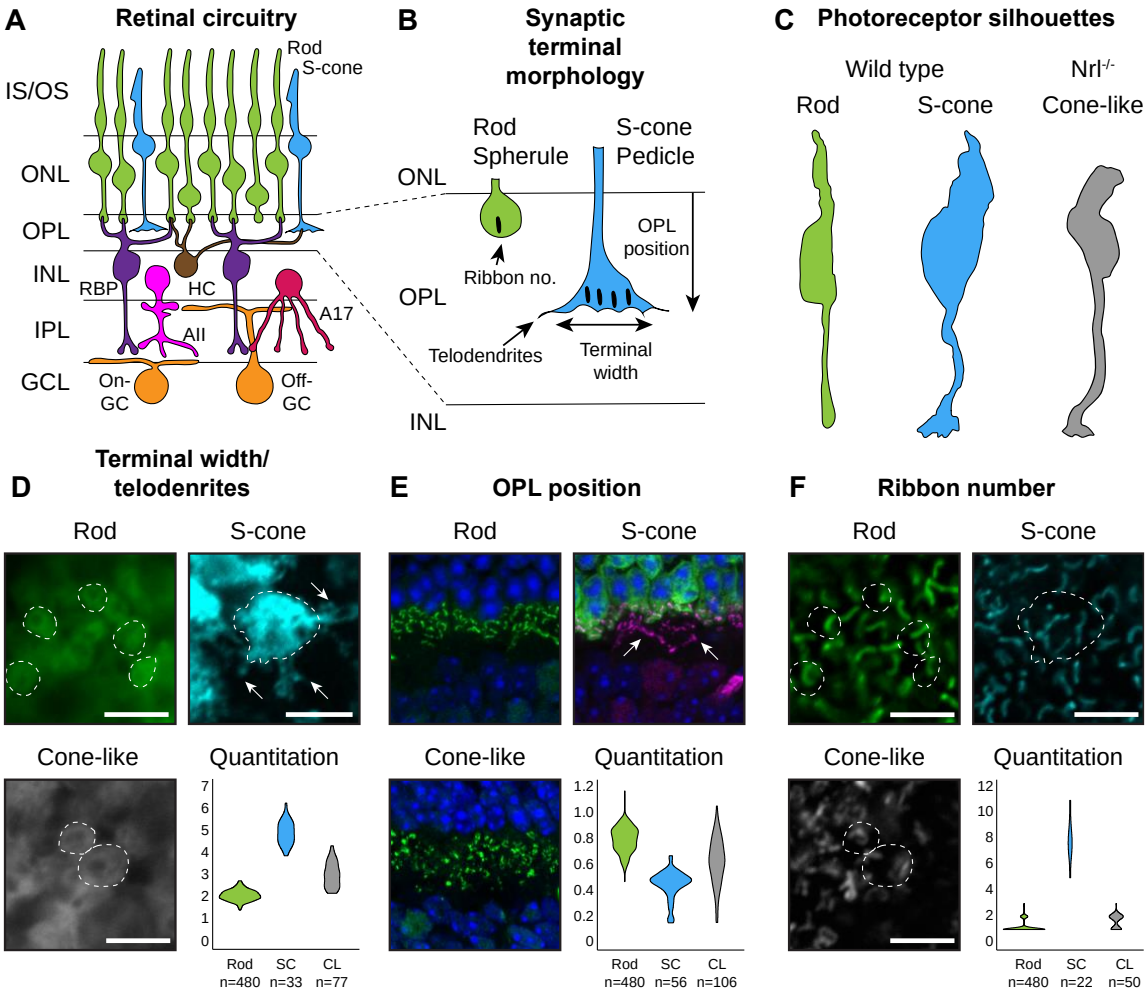

Figure 3. Photoreceptor terminal morphological features. (A) Schematic of retinal circuitry with both wild type photoreceptors shown (top). Some of the rod visual pathway is also represented. (B) Magnified view of the outer plexiform layer. Four features distinguish rod spherules from S-cone pedicles. (C) Silhouettes of wild type rod and S-cone and the *Nrl*-KO cone-like cells. (D) Diameter of photoreceptor terminals. Dotted lines indicate perimeter of terminal. Telodendrites are easily identifiable in S-cone pedicles (arrows). (E) Relative OPL position of photoreceptor terminals. Blue: DAPI; green/pink: ribeye antibody; arrows: cone ribbons. (F) Same terminals as seen in (D). Ribbon numbers counted within terminal (outline). All cone-like pedicles come from the *Nrl*$^{-/-}$ mouse line.

us with a solid baseline of the four rod and cone structural components so that we can detect deviations from the norm following genetic manipulation.

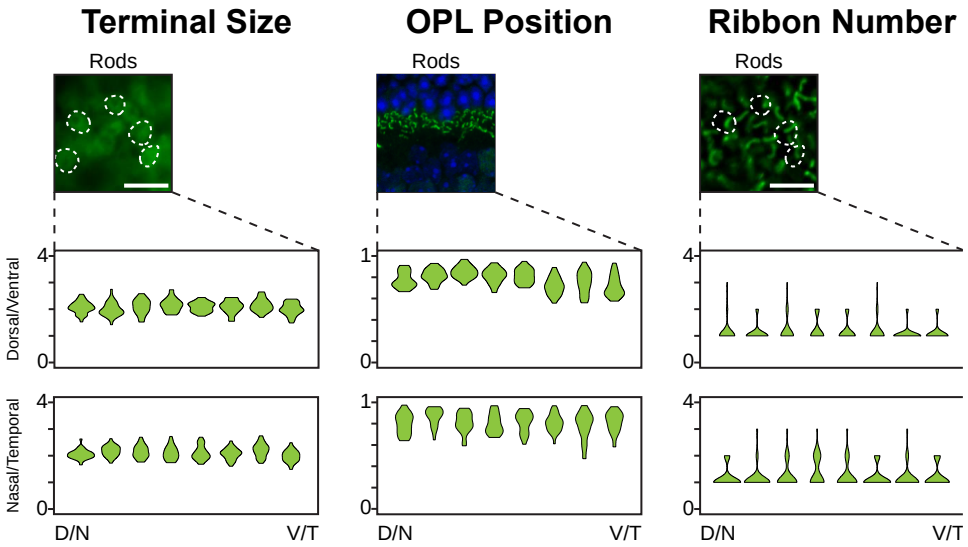

Figure 4. Spherule morphology along two retinal axes. Eight equidistant positions along two retinal axes were chosen for analysis of spherule position. No significant differences are detected between spherules in any position. (n=30 spherules/position. n=1 retina/structure/orientation (e.g. dorsal/ventral in terminal size).

Table 1. Spherule and pedicle structures. Listed are the compiled phenotypes described in the "Assay parameters to examine presynaptic structure" section (mean ± SEM; n=retina/terminals).

Phenotype	***Rod spherules***	***S-cone pedicles***	***Cone-like pedicles***
Terminal diameter	2.091 ± 0.011µm n = 2 / 480	4.917 ± 0.092µm n = 3 / 33	3.036 ± 0.063µm n = 3 / 77
Telodendrites	No	Yes: long	Yes: very short (not shown)
OPL position	0.796 ± 0.005 n = 2 / 480	0.449 ± 0.015 n = 2 / 55	0.628 ± 0.127 n = 2 / 50
Ribbon number median	1 n = 2 / 480	8 n = 2 / 22	2 n = 3 / 50

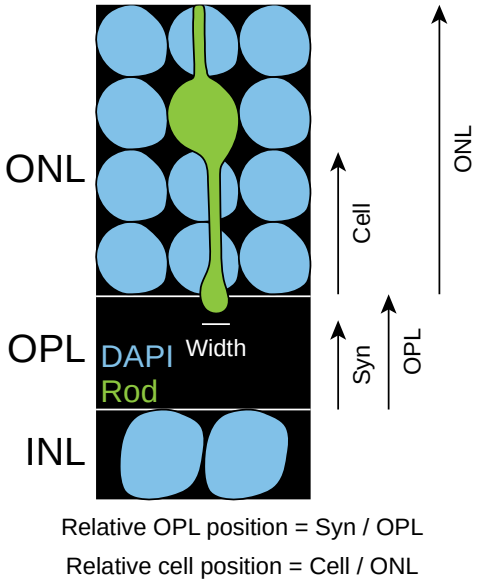

Figure 5. Schematic representation of quantitative measurements. Shown are how all screen images were quantified. “Cell” and “ONL” measurements were only collected for Figure 6.

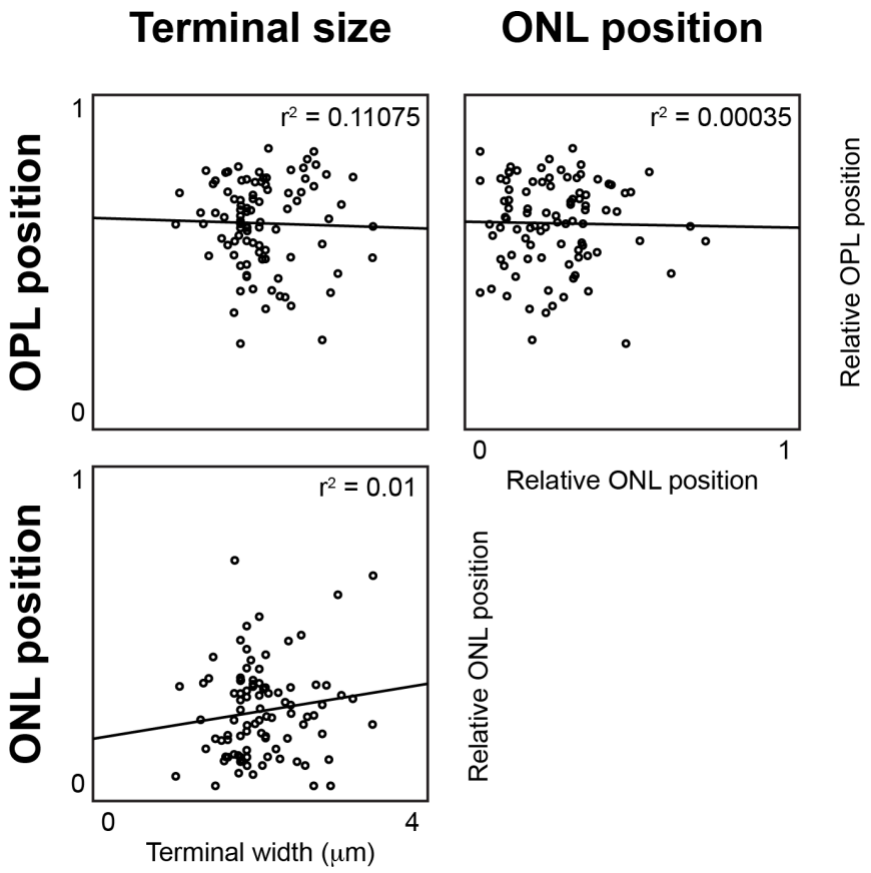

Figure 6. Spherule morphology from different layer rods. Pearson's correlation of values indicated at the top right of each graph. (top, left) Two of the four spherule phenotypes (those studied below) do not influence one another. (top, right and bottom, left) The rod photoreceptor cell body position within the ONL does not affect either spherule morphological feature.

Identification of candidate genes

To determine contributions of a subset of the NRL regulome to spherule morphology, we identified potential candidate genes that might be likely to be associated with the four above phenotypes. Rod photoreceptor structural maturation occurs between P6 – P10, with polarization and extension of neurites to make synaptic connections (Figure

7A); a sizable portion of the transcriptome also illustrates a sizeable shift in expression during this stage (Figure 7B; see also (Kim et al., 2016b)). Five filtering criteria were used to reduce our targeting gene pool using previously published RNA-sequencing transcriptome and ChIP-sequencing transcription factor binding data

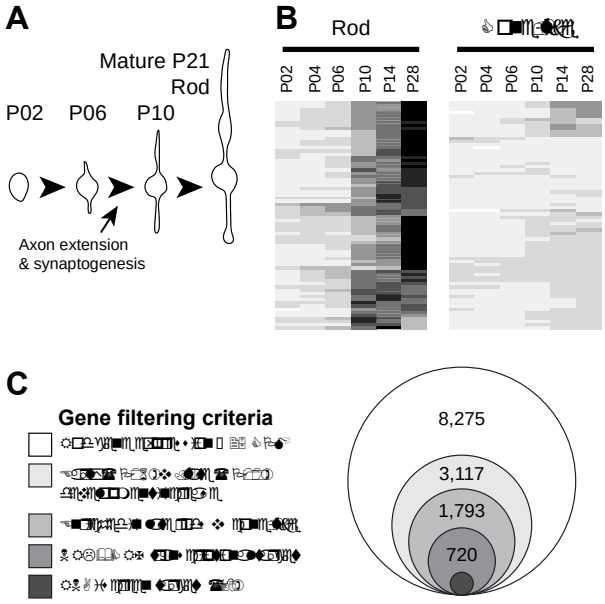

Figure 7. Gene candidate identification. (A) Schematic representation of rod photoreceptor structural maturation during postnatal development. Key period is between P6 – P10 when cell polarization and neurite extension occurs (arrow). (B) Postnatal developmental RNA-sequencing of rods and *Nrl*-KO cone-like cells. Heat map represents z-scores. Notice large shift in expression between P6 and P10 in rods but not in cone-like cells. (C) Gene filtering criteria to limit potential candidates from all rod transcriptome to a limited set of 78.

(Corbo et al., 2010; Hao et al., 2012; Kim et al., 2016b); the filters and resulting gene numbers can be seen in Figure 2C. (1) Genes expression was called if reached the highly

conservative 25 counts per million (CPM). (2) To capture the above shift in rod transcriptome, we only included genes increasing at least two-fold between early (P2 – 6) and late (P10 – 28) development. (3) We wanted to identify genes enriched in mature rods so only included genes enriched in late development rods compared to cone-like cells by two-fold. (4) As NRL and CRX are essential for rod photoreceptor spherule development, we used only genes containing experimentally-validated (ChIP-sequencing) transcription factor binding sites. These four filters gave us a narrower list of 720 genes. Our final filter (5) was to use a combination of gene ontology analysis to find enriched categories and manual curation to limit our targets to approximately 10% of the 720 (78 genes) (see absolute expression profiles in Figure 8). Now that genes were selected, we wanted to know their role in formation of spherule morphology. In our current study, we focused on how spherule morphological features were affected by reduction of gene expression through RNAi screening.

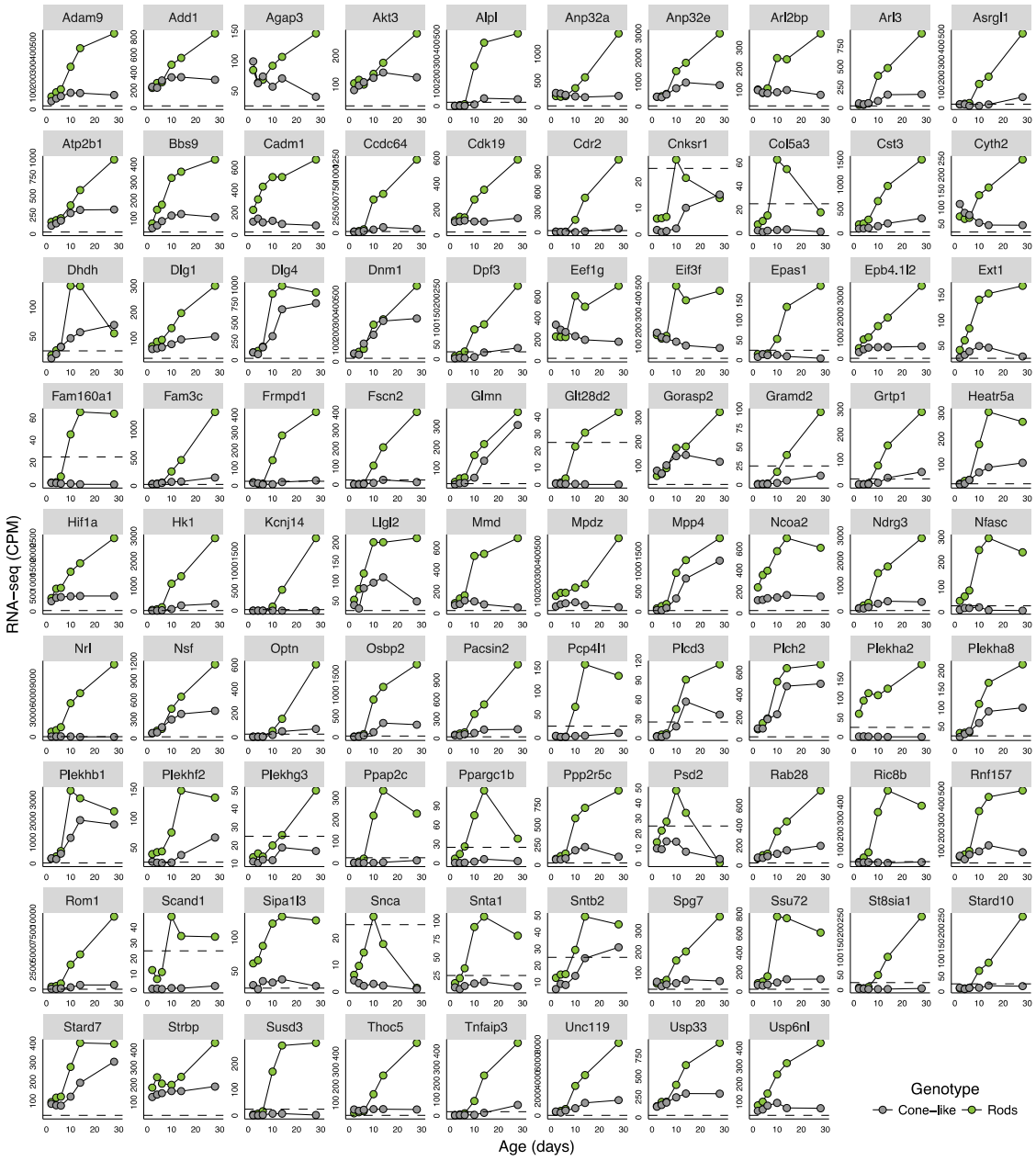

Figure 8. Candidate gene expression profiles. Individual expression profiles of all selected target genes. Note that most genes have a similar pattern with no/low expression between P2 – P6, have a drastic increase at P10, and expression tends to plateau at P10. Rod: green dots; cone-like cells: white dots; dashed line marks 25 CPM. Note that the y-axis scale, RNA-sequencing expression in CPM, differs in each graph. Each data point represents averaged gene expression of 2 – 4 replicates.

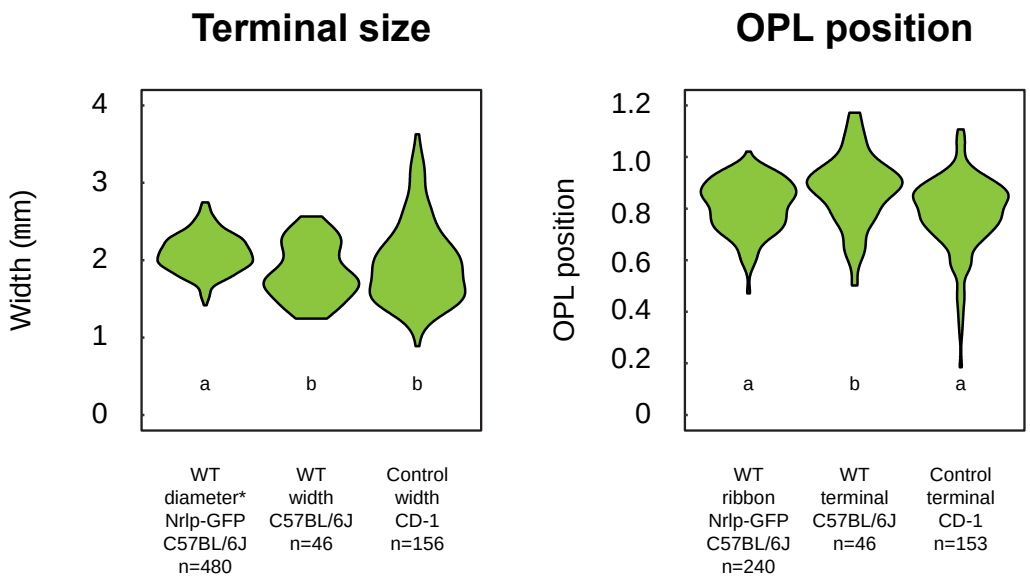

Figure 9. Spherule comparison between strains and methods. We investigated if spherule features resembled one another between our original C57BL/6J wild type and the CD-1® mouse strains used in our study. We also determined if method of investigation (transgenic, un-injected versus electroporated) biased quantitative measurements. Statistically different groups are represented by different letters under graph; if the letter is the same, the groups showed no average difference. Numbers indicate individual spherules. Each group contains spherules from ≥2 retinas.

RNAi screen for presynaptic terminal size

We initially focused on the distinct size between rod and cone terminals. We were curious if we could alleviate some restricting force from the spherules to allow enlarged pedicle-like terminal size. We performed *in vivo* electroporation of short hairpin RNAs (shRNAs) and fluorescent reporters at P0 – 1, prior to increases in gene expression, and assayed the width at P21 – 22, when spherules are matured. In this screen (Figure 10A), knockdown of 7 genes (Dpf3, Epb4.1l2, Grtp1, Kcnj14, Llgl2, Rab28, and Rom1) significantly increased the spherule morphology of rods (Table 3) (see examples in Figure

10B; Kruskal-Wallis one-way ANOVA with Dunn's test for multiple comparisons). The positive controls (two shRNAs against Nrl) showed increased sized spherules. While none of our knockdowns presented a true S-cone pedicle size, we did find two constructs (Kcnj14 and Llgl2) that gene reduction displayed terminals similar to cone-like pedicles ($p>0.1$). These data provide strong evidence for the hypothesis that NRL targets restrict spherule size, and lessening this restriction will enlarge spherule size towards that of pedicles (as in the case of our 7 positive hits).

RNAi screen for spherule OPL positioning

Our initial width screen also pointed to gene knockdown affecting where spherules lie in the OPL, so we also quantitatively addressed this feature. As in Figure 1E, we use a relative measurement to assay terminal localization with the OPL; unlike the previous data, here we use the bottom of the fluorescently-filled spherule. These two measurements are not significantly different ($p>0.5$; Figure 9), so we proceeded with this measurement in our screen. In the same terminals as above, we found that reduction of 23 genes (29%) affected OPL localization (Figure 11; Table 2). Unlike the spherule width phenotype above, this screen did identify 14 genes that led to patterns similar to native S-cones. Nine others deviated from rod spherule controls but lie intermediate between wild type rod and S-cone layers. Unexpectedly, within the 14 knockdown terminals with medians similar to S-cones, we found three (Arl2bp, Rom1, and St8sia1) that often completely bypassed the OPL, and terminals were often found extending into

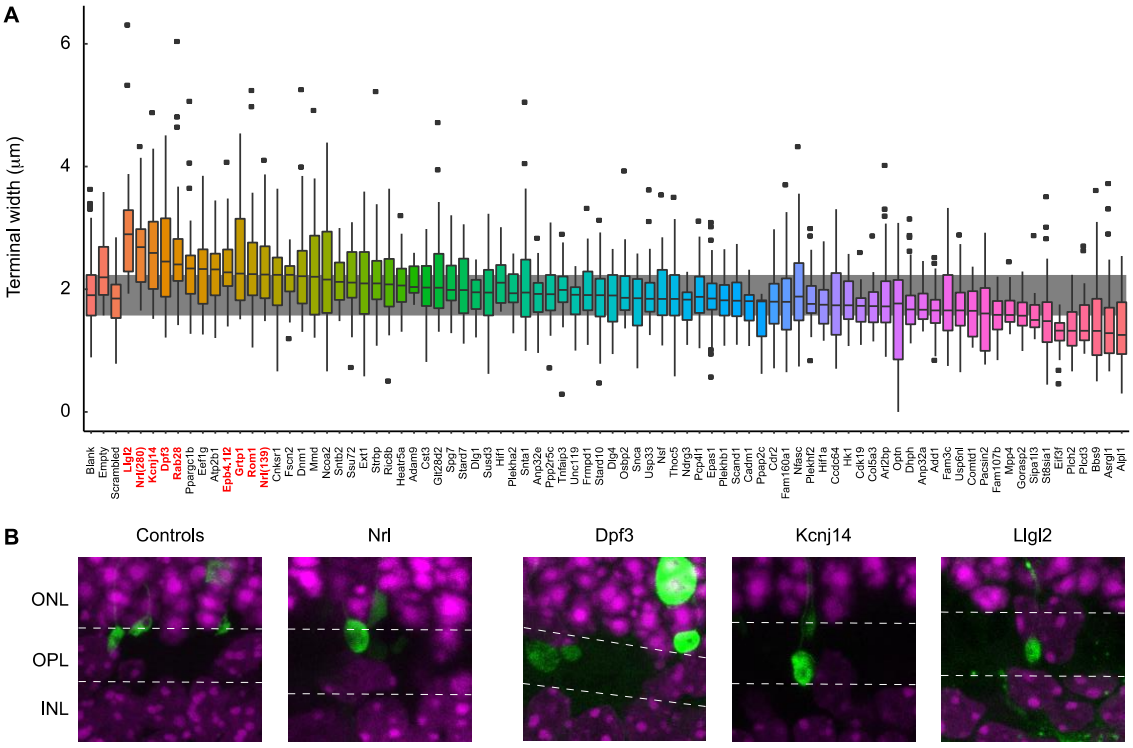

Figure 10. RNAi screen for terminal width phenotype. (A) Quantitative box plot of relative spherule Grey shaded area represents 25th-75th percentile of fluorescent reporter-only ("Blank") control. After negative controls, screen genes are ordered with largest median (most cone-like) on left. Colored gene names are statistically different than controls. Red gene names: significantly different than "Blank" control. (B) Example images of negative control, Nrl, and three positive screen hits are shown. Dotted lines indicate outer plexiform layer boundaries. Red

the inner nuclear layer (Figure 12). These data expand upon our list of genes associated with restriction of spherule morphology; we also found that four genes (Epb4.1l2, Kcnj14, Llgl2, and Rom1) have an effect on both features. Interestingly, other phenotypes emerged during our RNAi screen that are independent of spherule structure, including how the cell bodies are positioned in the ONL and DNA architecture is organized within the nucleus (Figure 12).

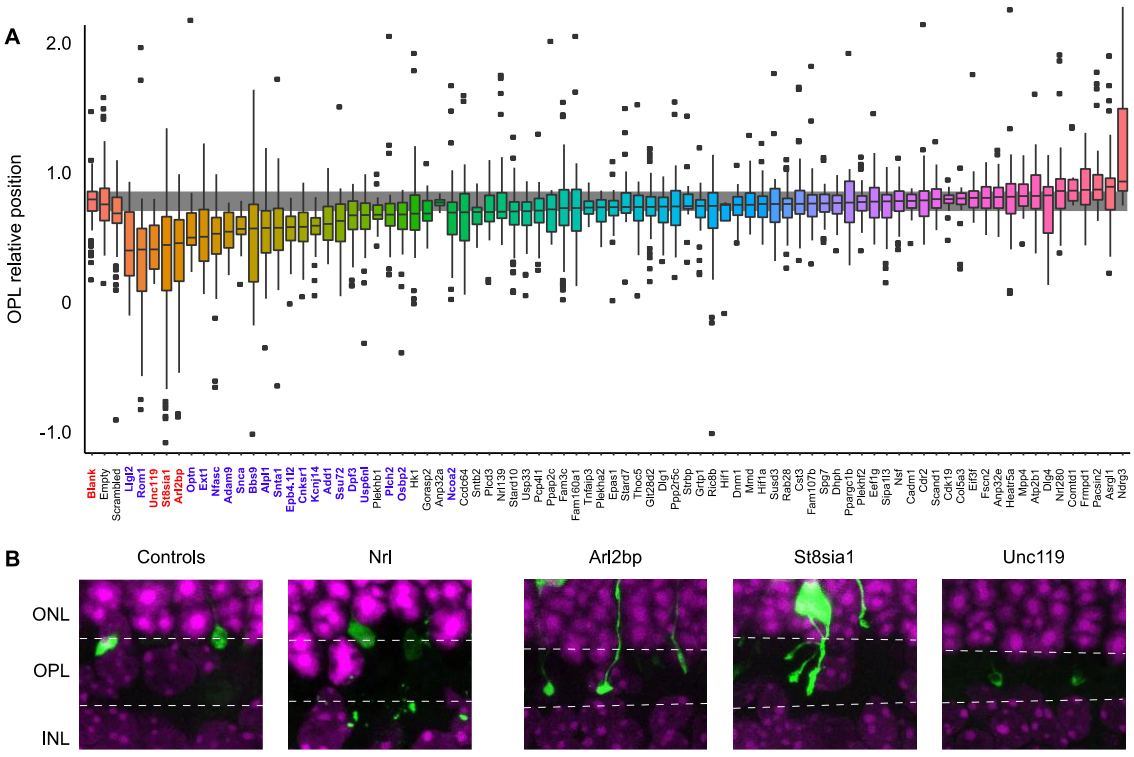

Figure 11. RNAi screen for OPL position phenotype. (A) Quantitative box plot of relative terminal OPL positioning (0: upper boundary of inner nuclear layer; 1: lower boundary of outer nuclear layer). Grey shaded area represents 25th-75th percentile of fluorescent reporter-only ("Blank") control. After negative controls, screen genes are ordered with lowest median OPL position on left. Colored gene names, minus Blank, are statistically different than controls. Red gene names: examples images in (B) and significantly different than the "Blank" control. Blue gene names: significantly different than the "Blank" control. (B) Example images of negative control, Nrl, and three positive screen hits are shown. Dotted lines indicate outer plexiform layer boundaries.

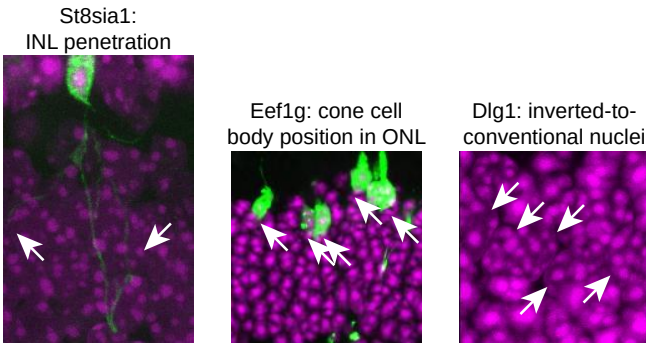

Figure 12. Additional phenotypes from RNAi screen. Here we see that additional phenotypes can be detected in our RNAi screen. (Left) St8sia1, and two others, often show a complete bypass of the OPL where axons extend into the INL (arrows). (Center) Rod cell bodies cover the entire ONL, and electroporated retinas tend to show distribution across this layer. Some knockdowns (i.e. Eef1g) had a tendency to have a more cone-like, upper ONL phenotype (arrows). (Right) Rods have an inverted nucleus (one large heterochromatin pocket in the middle) while cones have the conventional structure. One gene, Dlg1, was confirmed to affect this morphology.

Table 2. RNAi knockdown phenotypes. Listed are spherule features within each gene knockdown. Bolded numbers highlight statistical significance from Blank control. Any additional phenotypes (unconfirmed) are mentioned in the last column.

Gene name	**shRNA TRCN#**	**Retina no.**	**Width mean ± SEM Term. no. / p-value**	**OPL mean ± SEM Term. no. / p-value**	**Other notes**
Adam9	TRCN0000031817	n=2	2.130 ± 0.096 n=10 / p>0.9999	**0.550 ± 0.058 n=10 / p=0.0236**	
Add1	TRCN0000108809	n=1	1.683 ± 0.061 n=45 / p=0.2196	**0.633 ± 0.029 n=41 / p=0.0002**	

Table 2 Continued.

Gene name	**shRNA TRCN#**	**Retina no.**	**Width mean ± SEM Term. no. / p-value**	**OPL mean ± SEM Term. no. / p-value**	**Other notes**
Alpl1	TRCN0000081503	n=1	1.336 ± 0.092 n=34 / p<0.0001	**0.539 ± 0.049 n=34 / p<0.0001**	
Anp32e	TRCN0000311767	n=1	1.893 ± 0.083 n=28 / p>0.9999	0.830 ± 0.028 n=28 / p>0.9999	
Arl2bp	TRCN0000250373	n=1	1.830 ± 0.063 n=82 / p>0.9999	**0.381 ± 0.043 n=80 / p<0.0001**	
Asrgl1	TRCN0000032311	n=2	1.403 ± 0.087 n=55 / p<0.0001	0.915 ± 0.044 n=55 / p>0.9999	
Atp2b1	TRCN0000101642	n=1	2.265 ± 0.093 n=32 / p=0.3963	0.861 ± 0.040 n=32 / p>0.9999	
Bbs9	TRCN0000336347	n=2	1.407 ± 0.105 n=45 / p<0.0001	**0.514 ± 0.072 n=45 / p<0.0001**	
Blank		n=3	1.973 ± 0.042 n=155	0.786 ± 0.012 n=152	Negative control – comparison group
Cadm1	TRCN0000124315	n=1	1.735 ± 0.055 n=29 / p>0.9999	0.779 ± 0.017 n=29 / p>0.9999	
Ccdc64	TRCN0000265210	n=2	1.772 ± 0.097 n=47 / p>0.9999	0.708 ± 0.045 n=47 / p=0.2968	

Table 2 Continued.

Gene name	**shRNA TRCN#**	**Retina no.**	**Width mean ± SEM Term. no. / p-value**	**OPL mean ± SEM Term. no. / p-value**	**Other notes**
Cdk19	TRCN0000023283	n=1	1.693 ± 0.068 n=27 / p>0.9999	0.797 ± 0.016 n=27 / p>0.9999	
Cdr2	TRCN0000240531	n=1	1.777 ± 0.077 n=50 / p>0.9999	0.936 ± 0.127 n=50 / p>0.9999	
Cnksr1	TRCN0000362955	n=1	2.196 ± 0.104 n=37 / p>0.9999	**0.594 ± 0.031 n=37 / p<0.0001**	
Col5a3	TRCN0000089854	n=1	1.770 ± 0.085 n=22 / p>0.9999	0.773 ± 0.038 n=22 / p>0.9999	
Comtd1	TRCN0000097393	n=1	1.647 ± 0.153 n=10 / p>0.9999	0.950 ± 0.072 n=10 / p>0.9999	
Cst3	TRCN0000055249	n=2	2.038 ± 0.070 n=55 / p>0.9999	0.819 ± 0.033 n=55 / p>0.9999	
Dhdh	TRCN0000192341	n=1	1.805 ± 0.105 n=28 / p>0.9999	0.765 ± 0.024 n=28 / p>0.9999	
Dlg1	TRCN0000321863	n=1	1.897 ± 0.064 n=29 / p>0.9999	0.724 ± 0.031 n=29 / p>0.9999	Possible genome rearrangement
Dlg4	TRCN0000025482	n=1	1.861 ± 0.104 n=21 / p>0.9999	0.738 ± 0.061 n=21 / p>0.9999	

Table 2 Continued.

Gene name	**shRNA TRCN#**	**Retina no.**	**Width mean ± SEM Term. no. / p-value**	**OPL mean ± SEM Term. no. / p-value**	**Other notes**
Dnm1	TRCN0000349422	n=2	2.302 ± 0.098 n=54 / p=0.2792	0.752 ± 0.016 n=54 / p>0.9999	
Dpf3	TRCN0000086343	n=2	**2.575 ± 0.096 n=66 / p<0.0001**	**0.654 ± 0.024 n=64 / p=0.0007**	
Eef1g	TRCN0000245388	n=1	2.273 ± 0.112 n=29 / p>0.9999	0.807 ± 0.040 n=29 / p>0.9999	Possible cell body ONL positioning
Eif3f	TRCN0000265698	n=1	1.276 ± 0.070 n=21 / p<0.0001	0.850 ± 0.051 n=21 / p>0.9999	
Empty	SHC201	n=2	2.314 ± 0.096 n=31 / p=0.2108	0.8176 ± 0.060 n=31 / p>0.9999	Negative control
Epas1	TRCN0000416474	n=2	1.861 ± 0.075 n=46 / p>0.9999	0.733 ± 0.023 n=45 / p>0.9999	
Epb4.1l2	TRCN0000327110	n=1	**2.345 ± 0.080 n=41 / p=0.0086**	**0.575 ± 0.026 n=41 / p<0.0001**	
Ext1	TRCN0000313800	n=1	2.104 ± 0.123 n=31 / p>0.9999	**0.533 ± 0.048 n=31 / p<0.0001**	
Fam3c	TRCN0000292668	n=1	1.760 ± 0.084 n=57 / p>0.9999	0.716 ± 0.042 n=57 / p>0.9999	

Table 2 Continued.

Gene name	**shRNA TRCN#**	**Retina no.**	**Width mean ± SEM Term. no. / p-value**	**OPL mean ± SEM Term. no. / p-value**	**Other notes**
Fam160a1	TRCN0000182560	n=1	1.844 ± 0.146 n=26 / p>0.9999	0.787 ± 0.076 n=26 / p>0.9999	
Fam107b	TRCN0000192096	n=1	1.592 ± 0.044 n=49 / p=0.0021	0.775 ± 0.032 n=49 / p>0.9999	
Frmpd1	TRCN0000255539	n=1	1.988 ± 0.089 n=30 / p>0.9999	0.878 ± 0.038 n=30 / p>0.9999	
Fscn2	TRCN0000436775	n=1	2.182 ± 0.079 n=29 / p>0.9999	0.828 ± 0.028 n=26 / p>0.9999	
Glt28d2	TRCN0000432398	n=1	2.203 ± 0.115 n=40 / p>0.9999	0.742 ± 0.036 n=40 / p>0.9999	
Gorasp2	TRCN0000077520	n=1	1.603 ± 0.057 n=29 / p=0.0704	0.714 ± 0.024 n=29 / p>0.9999	
Grtp1	TRCN0000106225	n=1	**2.545 ± 0.148 n=34 / p=0.0383**	0.716 ± 0.033 n=34 / p>0.9999	
Heatr5a	TRCN0000249612	n=1	2.102 ± 0.079 n=31 / p>0.9999	0.827 ± 0.067 n=31 / p>0.9999	
Hif1a	TRCN0000232222	n=1	1.822 ± 0.084 n=28 / p>0.9999	0.752 ± 0.046 n=27 / p>0.9999	

Table 2 Continued.

Gene name	**shRNA TRCN#**	**Retina no.**	**Width mean ± SEM Term. no. / p-value**	**OPL mean ± SEM Term. no. / p-value**	**Other notes**
Hk1	TRCN0000012531	n=1	1.792 ± 0.065 n=46 / p>0.9999	0.726 ± 0.051 n=46 / p=0.2018	
Kcnj14	TRCN0000427941	n=1	**2.701 ± 0.155 n=31 / p=0.0012**	**0.571 ± 0.029 n=31 / p<0.0001**	
Llgl2	TRCN0000087880	n=1	**3.023 ± 0.211 n=24 / p<0.0001**	**0.459 ± 0.061 n=24 / p<0.0001**	
Mmd	TRCN0000326935	n=1	2.389 ± 0.179 n=26 / p>0.9999	0.838 ± 0.071 n=26 / p>0.9999	
Mpp4	TRCN0000362170	n=1	1.656 ± 0.054 n=29 / p=0.2824	0.842 ± 0.028 n=29 / p>0.9999	
Ncoa2	TRCN0000238244	n=1	2.281 ± 0.127 n=51 / p>0.9999	**0.576 ± 0.086 n=51 / p=0.0019**	
Ndrg3	TRCN0000200080	n=1	1.719 ± 0.063 n=26 / p>0.9999	1.266 ± 0.144 n=21 / p=0.0246	
Nfasc	TRCN0000094170	n=1	1.939 ± 0.085 n=66 / p>0.9999	**0.505 ± 0.041 n=58 / p<0.0001**	Elaborate axonal projections
Nrl (139)	TRCN0000085139	n=1	**2.385 ± 0.099 n=45 / p=0.0342**	0.804 ± 0.044 n=45 / p>0.9999	Positive control

Table 2 Continued.

Gene name	**shRNA TRCN#**	**Retina no.**	**Width mean ± SEM Term. no. / p-value**	**OPL mean ± SEM Term. no. / p-value**	**Other notes**
Nrl (280)	TRCN0000432280	n=1	**2.641 ± 0.088 n=51 / p<0.0001**	0.890 ± 0.041 n=51 / p>0.9999	Positive control
Nsf	TRCN0000323688	n=1	1.944 ± 0.084 n=38 / p>0.9999	0.776 ± 0.024 n=38 / p>0.9999	
Optn	TRCN0000177380	n=1	1.775 ± 0.206 n=12 / p>0.9999	**0.658 ± 0.136 n=13 / p=0.0151**	
Osbp2	TRCN0000438055	n=1	1.957 ± 0.078 n=38 / p>0.9999	**0.634 ± 0.038 n=38 / p=0.0065**	
Pacsin2	TRCN0000305724	n=2	1.618 ± 0.127 n=25 / p>0.9999	0.996 ± 0.064 n=25 / p=0.7137	
Pcp4l1	TRCN0000254700	n=1	1.890 ± 0.055 n=66 / p>0.9999	0.755 ± 0.050 n=63 / p=0.3329	
Plcd3	TRCN0000097070	n=1	1.486 ± 0.069 n=37 / p<0.0001	0.720 ± 0.031 n=37 / p>0.9999	
Plch2	TRCN0000452720	n=1	1.369 ± 0.061 n=43 / p<0.0001	**0.706 ± 0.044 n=43 / p=0.0211**	
Plekha2	TRCN0000174698	n=1	1.992 ± 0.079 n=20 / p>0.9999	0.710 ± 0.029 n=20 / p>0.9999	

Table 2 Continued.

Gene name	**shRNA TRCN#**	**Retina no.**	**Width mean ± SEM Term. no. / p-value**	**OPL mean ± SEM Term. no. / p-value**	**Other notes**
Plekhb1	TRCN0000111591	n=1	1.860 ± 0.085 n=26 / p>0.9999	0.701 ± 0.023 n=25 / p=0.4683	
Plekhf2	TRCN0000241277	n=1	1.858 ± 0.058 n=54 / p>0.9999	0.786 ± 0.017 n=54 / p>0.9999	
Ppap2c	TRCN0000081457	n=2	1.493 ± 0.191 n=7 / p>0.9999	0.859 ± 0.203 n=7 / p>0.9999	
Ppargc1b	TRCN0000366320	n=1	2.481 ± 0.211 n=19 / p>0.9999	0.984 ± 0.147 n=19 / p>0.9999	
Ppp2r5c	TRCN0000080548	n=1	1.952 ± 0.061 n=61 / p>0.9999	0.748 ± 0.029 n=61 / p>0.9999	
Rab28	TRCN0000100699	n=2	**2.576 ± 0.112 n=55 / p<0.0001**	0.741 ± 0.022 n=54 / p>0.9999	Possible genome rearrangement
Ric8b	TRCN0000445620	n=2	2.137 ± 0.078 n=55 / p>0.9999	0.669 ± 0.048 n=55 / p>0.9999	
Rom1	TRCN0000314121	n=1	**2.356 ± 0.071 n=93 / p=0.0009**	**0.324 ± 0.048 n=90 / p<0.0001**	
Scand1	TRCN0000257136	n=1	1.872 ± 0.089 n=25 / p>0.9999	0.817 ± 0.031 n=25 / p>0.9999	

Table 2 Continued.

Gene name	**shRNA TRCN#**	**Retina no.**	**Width mean ± SEM Term. no. / p-value**	**OPL mean ± SEM Term. no. / p-value**	**Other notes**
Scrambled	SHC202	n=3	1.819 ± 0.051 n=75 / p>0.9999	0.7298 ± 0.031 n=74 / p>0.9999	Negative control
Sipa1l3	TRCN0000106037	n=1	1.664 ± 0.087 n=30 / p=0.0868	0.720 ± 0.040 n=29 / p>0.9999	
Snca	TRCN0000377011	n=1	1.793 ± 0.074 n=40 / p>0.9999	**0.583 ± 0.020 n=41 / p<0.0001**	
Snta1	TRCN0000108644	n=2	2.102 ± 0.097 n=64 / p>0.9999	**0.573 ± 0.039 n=63 / p<0.0001**	
Sntb2	TRCN0000112917	n=1	2.140 ± 0.069 n=31 / p>0.9999	0.689 ± 0.021 n=31 / p=0.1289	
Spg7	TRCN0000031204	n=1	2.083 ± 0.069 n=44 / p>0.9999	0.767 ± 0.022 n=41 / p>0.9999	
Ssu72	TRCN0000111980	n=1	2.164 ± 0.100 n=31 / p>0.9999	**0.614 ± 0.051 n=31 / p=0.0012**	
St8sia1	TRCN0000110307	n=2	1.472 ± 0.046 n=125 / p<0.0001	**0.214 ± 0.064 n=125 / p<0.0001**	Bypasses OPL in many examples
Stard7	TRCN0000105121	n=1	2.206 ± 0.122 n=21 / p>0.9999	0.813 ± 0.060 n=21 / p>0.9999	

Table 2 Continued.

Gene name	**shRNA TRCN#**	**Retina no.**	**Width mean ± SEM Term. no. / p-value**	**OPL mean ± SEM Term. no. / p-value**	**Other notes**
Stard10	TRCN0000105062	n=3	1.865 ± 0.038 n=159 / p>0.9999	**0.691 ± 0.014 n=157 / p=0.0001**	
Strbp	TRCN0000086391	n=1	2.316 ± 0.267 n=14 / p>0.9999	0.792 ± 0.069 n=14 / p>0.9999	
Suds3	TRCN0000247409	n=1	1.932 ± 0.102 n=34 / p>0.9999	0.826 ± 0.068 n=34 / p>0.9999	
Thoc5	TRCN0000123772	n=1	1.886 ± 0.071 n=63 / p>0.9999	0.955 ± 0.168 n=63 / p>0.9999	
Tnfaip3	TRCN0000378470	n=1	2.128 ± 0.128 n=15 / p>0.9999	0.740 ± 0.025 n=14 / p>0.9999	
Unc119	TRCN0000177275	n=1	1.783 ± 0.084 n=23 / p>0.9999	**0.435 ± 0.041 n=23 / p<0.0001**	
Usp6nl	TRCN0000086812	n=1	1.728 ± 0.063 n=61 / p=0.5140	**0.631 ± 0.041 n=60 / p=0.0012**	
Usp33	TRCN0000030822	n=2	1.890 ± 0.045 n=781 / p>0.9999	**0.679 ± 0.018 n=78 / p=0.0021**	

Rescuing spherule morphology

We sought to validate our screen and reject type I errors from the above results. The "gold standard" of RNAi validation requires rescue of the original phenotype by re-introduction of the targeted gene's cDNA. We obtained cDNAs for nine of our positive genes (split between both phenotypes), altered the shRNA-binding sites by creating synonymous alterations (Figure 13), and injected these alongside the shRNA. If the control spherule phenotype is rescued, the targeted gene is responsible for the seen phenotype. For terminal width, re-introduction of the cDNA restricted three spherules back to wild type levels (Dpf3, Kcnj14, and Rab28) and enlarged one that by knockdown was smaller (St8sia1) (Figure 14A). Rescue experiments for OPL positioning recovered normal lamination patterns in five cases (Arl2bp, Ext1, Kcnj14, Snta1, and St8sia1) (Figure 14B). Two knockdowns (Dpf3 and Unc119) are possibly due to an off-target gene because of lack of full recovery; one of these two (Unc119) does show partial recovery, so gene expression levels might need to be increased for full recovery. Overall, we show that by adding the original gene alongside our shRNAs we are able to recover 9 of 11 spherule morphology alterations. These data provide us with high confidence that the data found in our two RNAi screens are reliable, with some limited exceptions.

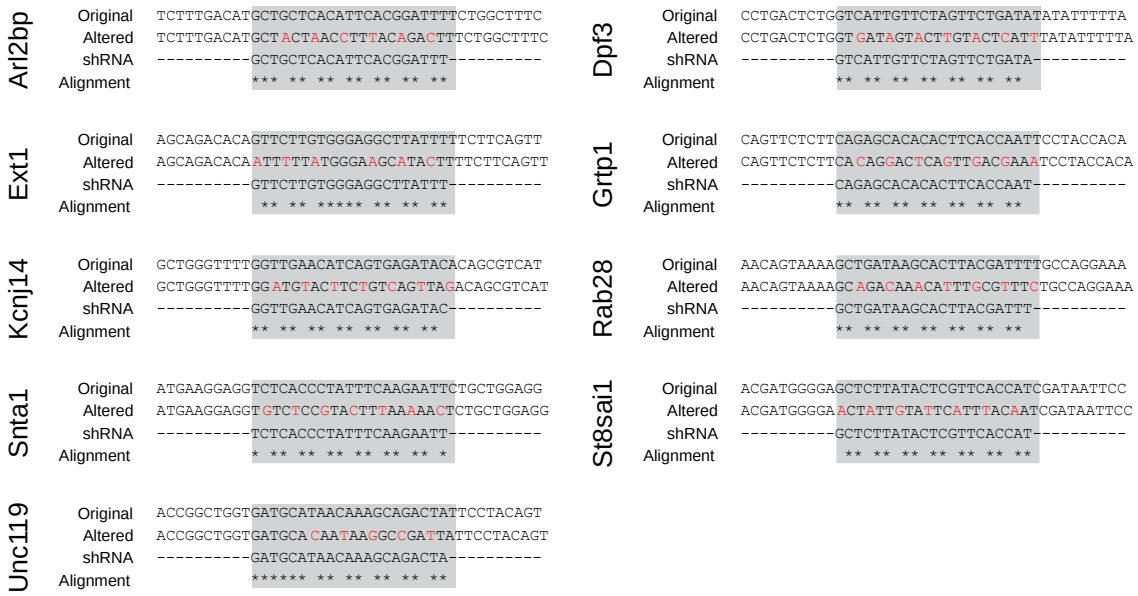

Figure 13. Codon-altered cDNAs for rescue. Sequence flanking shRNA-binding site is shown for each gene. Highlighted in grey is the shRNA-binding site. For altered cDNAs, wobble nucleotide altered to change nucleotide sequence without a resulting amino acid change. In each cDNA, 5 – 7 nucleotides were altered to lessen shRNA's ability to knockdown gene expression.

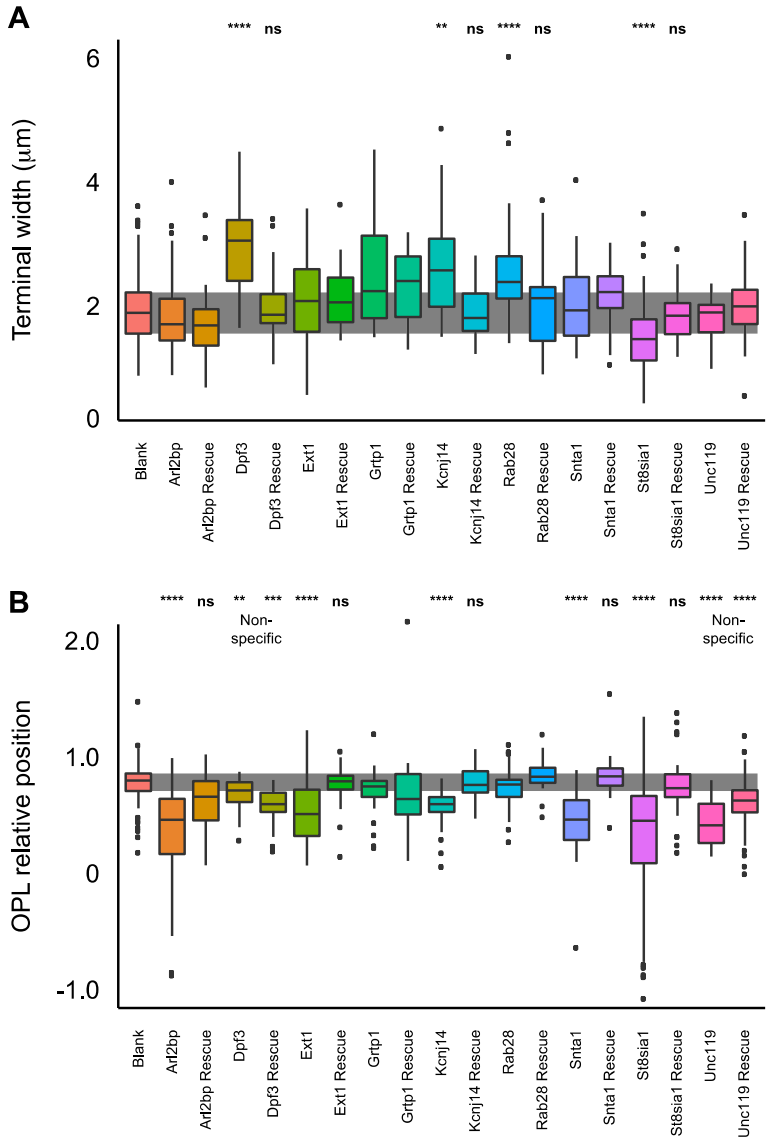

Figure 14. Rescue of knockdown morphology. Codon-altered cDNAs were injected alongside shRNA and quantified. Blank negative control on left. Grey bar represents 25th-75th percentile of control. Knockdowns and rescues are ordered alphabetically. (A) Re-introduction of gene rescued 4 out of 4 spherule size alterations. (B) OPL position rescued in 5 out of 7 knockdowns. Dpf3 looks to have a non-specific effect; Unc119 gave partial, non-significant rescue.

Table 3. Codon-altered knockdown rescue. Listed are spherule features within each gene knockdown. Bolded numbers highlight statistically significant.

Gene name	**shRNA TRCN#**	**Retina no.**	**Width mean ± SEM Term. no. / p-value**	**OPL mean ± SEM Term. no. / p-value**	**Other notes**
Blank		n=3	1.973 ± 0.042 n=155	0.786 ± 0.012 n=152	Negative control – comparison group
Arl2bp	TRCN0000250373	n=1	1.830 ± 0.063 n=82 / p>0.9999	**0.381 ± 0.043 n=80 / p<0.0001**	
Arl2bp - Rescue		n=1	1.767 ± 0.131 n=23 / p>0.9999	0.623 ± 0.050 n=23 / p=0.097	
Dpf3	TRCN0000086343	n=2	**2.575 ± 0.096 n=66 / p<0.0001**	**0.654 ± 0.024 n=64 / p=0.0007**	
Dpf3 – Rescue		n=1	1.987 ± 0.096 n=34 / p>0.9999	0.593 ± 0.024 n=29 / p=0.0001	
Ext1	TRCN0000313800	n=1	2.104 ± 0.123 n=31 / p>0.9999	**0.533 ± 0.048 n=31 / p<0.0001**	
Ext1 – Rescue		n=1	2.141 ± 0.078 n=37 / p>0.9999	1.116 ± 0.247 n=37 / p>0.9999	
Grtp1	TRCN0000106225	n=1	**2.545 ± 0.148 n=34 / p=0.0383**	0.716 ± 0.033 n=34 / p>0.9999	

Table 3 Continued.

Gene name	**shRNA TRCN#**	**Retina no.**	**Width mean ± SEM Term. no. / p-value**	**OPL mean ± SEM Term. no. / p-value**	**Other notes**
Grtp1 – Rescue		n=1	2.322 ± 0.103 n=29 / p=0.7960	0.677 ± 0.056 n=29 / p=0.3878	
Kcnj14	TRCN0000427941	n=1	**2.701 ± 0.155 n=31 / p=0.0012**	**0.571 ± 0.029 n=31 / p<0.0001**	
Kcnj14 – Rescue		n=1	1.908 ± 0.078 n=27 / p>0.9999	0.784 ± 0.027 n=27 / p>0.9999	
Rab28	TRCN0000100699	n=2	**2.576 ± 0.112 n=55 / p<0.0001**	0.741 ± 0.022 n=54 / p>0.9999	Possible genome rearrangement
Rab28 – Rescue		n=1	2.080 ± 0.146 n=29 / p>0.9999	0.893 ± 0.022 n=29 / p>0.9999	
Snta1	TRCN0000108644	n=2	2.102 ± 0.097 n=64 / p>0.9999	**0.573 ± 0.039 n=63 / p<0.0001**	
Snta1 – Rescue		n=1	2.193 ± 0.088 n=28 / p>0.9999	0.839 ± 0.036 n=28 / p>0.9999	
St8sia1	TRCN0000110307	n=2	1.472 ± 0.046 n=125 / p<0.0001	**0.214 ± 0.064 n=125 / p<0.0001**	Bypasses OPL in many examples
St8sia1 – Rescue		n=1	1.860 ± 0.082 n=29 / p>0.9999	0.760 ± 0.053 n=29 / p>0.9999	

Table 3 Continued.

Gene name	**shRNA TRCN#**	**Retina no.**	**Width mean ± SEM Term. no. / p-value**	**OPL mean ± SEM Term. no. / p-value**	**Other notes**
Unc119	TRCN0000177275	n=1	1.783 ± 0.084 n=23 / p>0.9999	**0.435 ± 0.041 n=23 / p<0.0001**	
Unc119 – Rescue		n=1	2.043 ± 0.068 n=53 / p>0.9999	0.619 ± 0.032 n=53 / p<0.0001	Partial recovery

Protein network predicts novel pathways for spherule morphology

We verified that our RNAi screen data is reliable, so we wanted to identify if our experimentally-validated genes could help predict new, high-confidence targets for future analysis. We created a first order neighbor network of our initial set of 720 genes, from high confidence protein interaction (score > 700) information described in STRING (Szklarczyk et al., 2017). The result was a massive network with 7,501 proteins sharing 28,419 interactions. This network was clustered into 176 communities with a minimum membership of 2 genes and maximum of 1485 (average 43) (Figure 15), but we found no significantly enrichment of our positive target genes into any cluster. Highlighting the validity of this clustering approach, though, cluster 24 contained 2 genes found to be positive regulators of synapse morphology (Nrl and Rom1) with 9 additional genes from our original list of 720 (Figure 7) and 41 additional members. These genes were enriched for the phototransduction pathway.

We used this large network to identify all the shortest paths connecting the positive targets (see Figure 16A for network flow chart), hoping to investigate the series of interactions necessary to attain the desired phenotype. The positive candidates appeared to be very well connected, resulting in more than 10,000 unique shortest paths between them. For the present study, we prioritized the shortest paths to enclose at least one other positive candidate, while not containing any experimentally verified negative targets. Only 104 paths (Figure 16B) qualified our stringent filter, encompassing a total of 83 proteins of which ~29% were experimentally verified positive candidates. Two interesting observations were immediately evident from this sets of connections: (1) Nrl, the center of our original GRN, is only represented in a single path, and (2) Ncoa2 and Dpf3 were both involved in >25% of all pathways. The pathway network centered around Ncoa2 (Figure 16C). Our protein interaction network analysis suggests several new candidates that have interesting functions in photoreceptors, which can be investigated in the future for their involvement in spherule morphogenesis (Figure 16C). From these data, we generated a novel hypothesis where there are tiers of regulation controlling spherule morphology, which begins with Nrl, is mediated by Ncoa2, and more direct affectors control spherule morphology (Figure 16D).

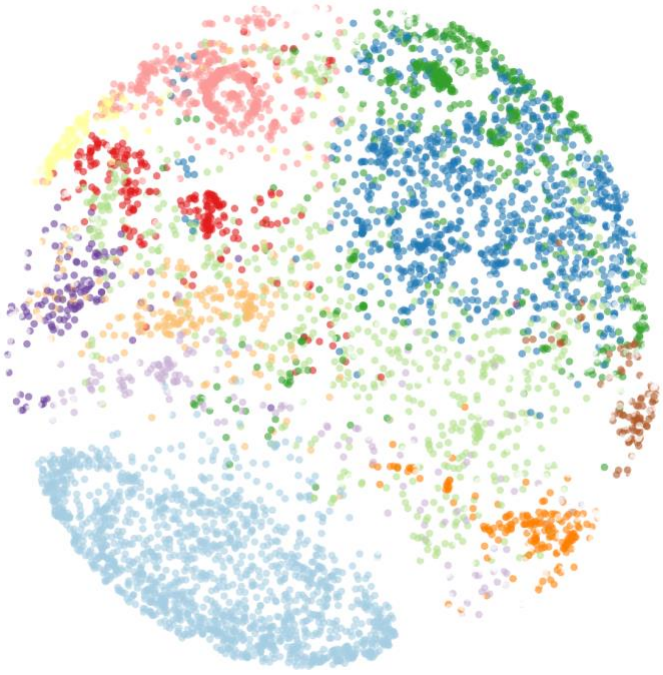

Figure 15. Protein interaction network: communities. Clustering the protein-protein interaction network separates all 7,501 proteins into 176 communities. The colors indicate membership in 1 of the 12 largest communities. There was no significant enrichment of our positive screen candidates in any community.

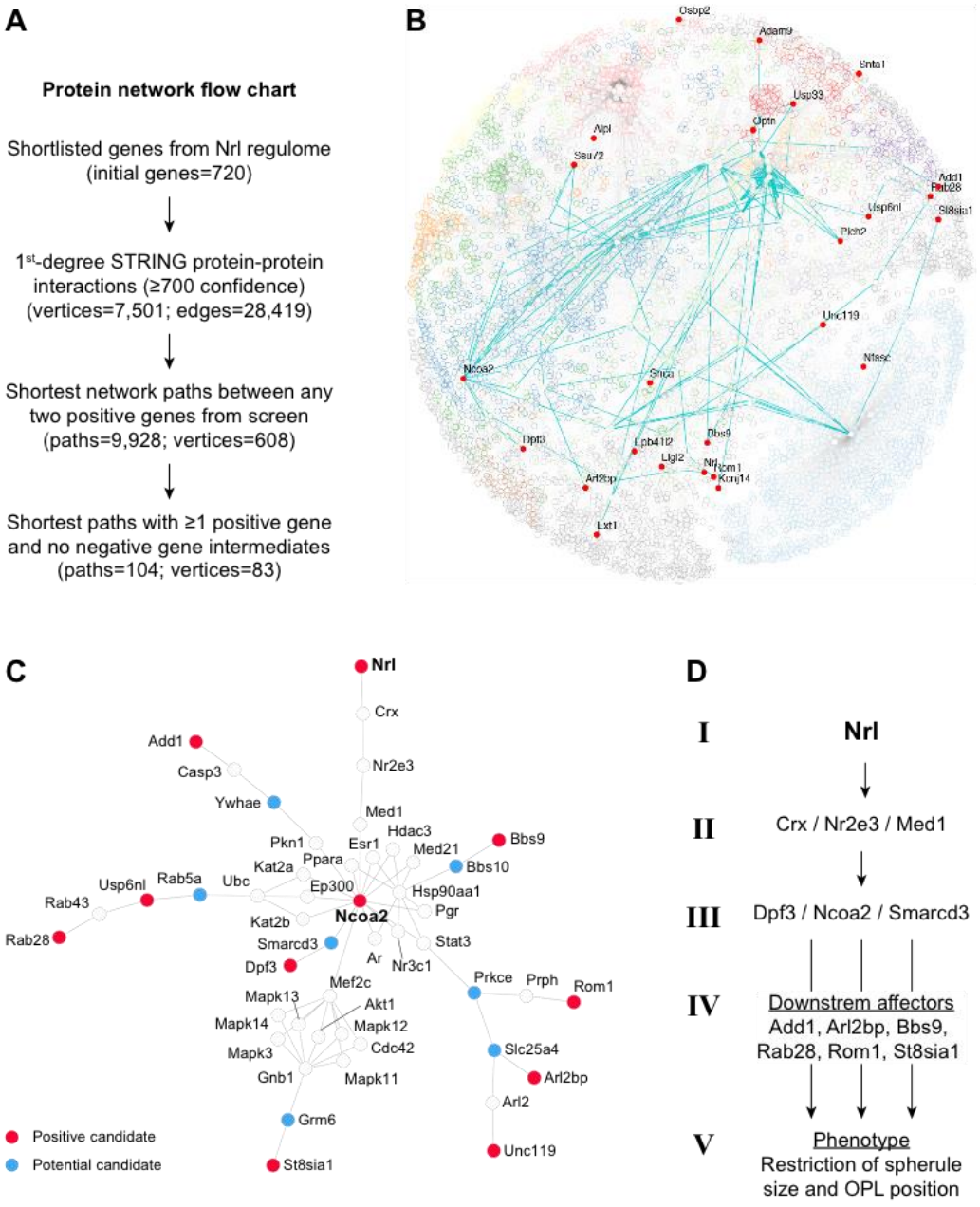

Figure 16. Shortest molecular paths between positive hits. (A) Analysis work flow. (B) Final 104 shortest positive-positive-positive pathways between screen targets overlaid on full protein-protein interaction. (C) Ncoa2 is located centrally in network pathways between Nrl and other positively screened genes. (D) New tiered hypothesis for Nrl-regulated spherule morphogenesis. Nrl lies at the top tier (I) of the network working through many determinants to affect spherule morphology (V)

Loss of function recapitulates spherule width phenotypes

Most RNAi knockdowns complement data found in knockout models, though this is not always the case (Baek et al., 2014), so we wanted to determine in our system if the two would match or show similar trends. We obtained two readily-available mouse strains, Epb4.1l2 and Snta1 (Adams et al., 2000; Sanuki et al., 2015), and generated AAV8-packaged CRISPR/Cas9 guides against two more, Dpf3 and Llgl2. We assayed these spherules as above at P21 with wild type/control CRISPR littermates as controls. Rod photoreceptors in all four null lines had significantly/trending larger terminals (Figure 17). Snta1 reduction in our RNAi screen did not show increased spherule size (Figure 10A) but complete loss was significantly enlarged (Figure 17). We increased our sample size of Snta1 shRNA and controls and did find that loss of Snta1 did shift terminal size towards that of pedicles (data not shown). The OPL lamination of all knockout models retained the control levels (data not shown). One of the two phenotypes (terminal width) from our RNAi screens is recapitulated by constitutive null models, and use of these models could be useful in determining how terminal size affects rod photoreceptor transmission.

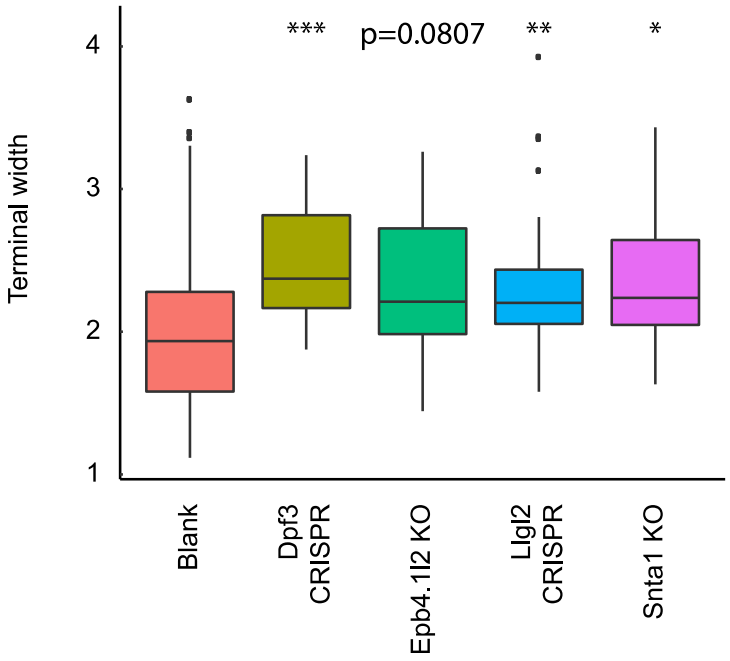

Figure 17. Loss of function spherule morphology. Terminal width of four loss of function mouse models. Two germline transgenic models (Epb4.1l2 and Snta1) and two CRISPR/Cas9-mediated knockout (Dpf3 and Llgl2) through AAV delivery.

Table 4. Spherule widths in loss of function retina.

Gene name	***Width mean ± SEM*** ***Term. no. / p-value***	***Other notes***
Blank	1.973 ± 0.042 n=155 /	Negative control – comparison group
Dpf3 – CRISPR	**2.458 ± 0.074** **n=26 / p=0.0006**	
Epb4.1l2 – KO	2.303 ± 0.089 n=27 / p=0.0807	
Llgl2 – CRISPR	**2.297 ± 0.058** **n=56 / p=0.0067**	
Snta1 – KO	**2.354 ± 0.092** **n=28 / p=0.0161**	

Enhanced neurotransmission with enlarged spherules

The relationship between neuronal structure and function is still an open question in neurobiology, with limited data supporting the hypothesis that larger axons and axon boutons can transmit greater signals. The loss of function animals we tested above provide a good system to directly compare how spherule (bouton) size affects neurotransmission. We hypothesized that loss of function animals with larger spherules would have a larger scotopic b-wave (indicative of rod-to-rod ON bipolar neurotransmission) without similar increases in scotopic a-waves (rod phototransduction) or photopic b-waves (cone-to-ON cone bipolar neurotransmission). We assayed one strain from above, the Snta1 knockout animal. As predicted, loss of function rod photoreceptors had greater neurotransmission to their bipolar cells (Figure 18, center) without a corresponding increase in incoming or detected signal (Figure 18, left). Cone to ON-bipolar transmission was unaffected in the knockout mice (Figure 18, right). These data show that enlarged synaptic terminals provide greater neurotransmission to postsynaptic cells in at least one model.

Discussion

Each neuronal class have both intrinsic genetic program and extrinsic signaling for maturation. Rod photoreceptor cell fate is controlled by the transcription factor Nrl to deviate away from the default S-cone program. This induction of Nrl initiates a cascade of events that lead to the large structural and functional differences between the two classes of photoreceptors. The restriction of spherule size and regulation of axon position in the OPL are controlled through unknown mechanisms. Axon size is important for strength of signal transmitted, and proper localization of terminals correctly places

spherules to contact appropriate interneurons. In the current study, we tested the hypothesis that a portion of the Nrl gene regulatory network actively modifies spherule morphology by precisely dissecting many genes' roles in controlling spherule structure in rod photoreceptors.

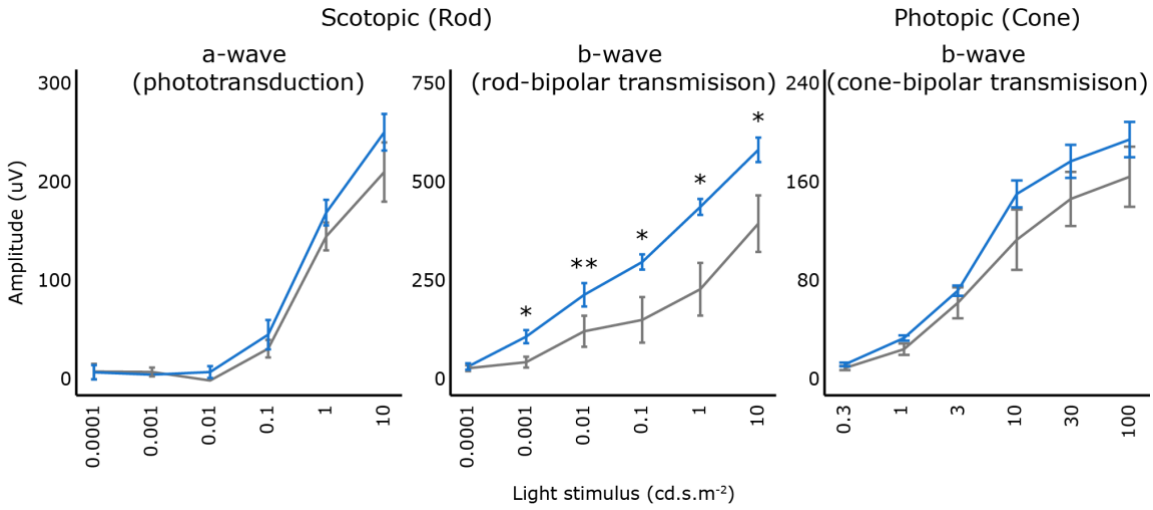

Figure 18. Enhanced neurotransmission with Snta1 loss of function. (left) The rod photoreceptor intrinsic response (phototransduction; a-wave) is not altered between heterozygous (grey) and knockout (blue) animals at any light intensity. Transmission between rods and ON-bipolar cells (b-wave) is enhanced at most light intensities (center); similar neurotransmission from cones is unaffected (right).

Through our RNAi screen, we discovered that knockdown of 27 genes controlled one or two of the independent features differentiating rod spherules versus cone pedicles. Seven genes in our screen controlled spherule width. Not one, though, showed a similar size to that found in S-cones, but did show similar to cone-like photoreceptors. We would predict that there are three factors that could cause smaller spherules that S-cone pedicles in our study: (1) there is not sufficient space in an already crowded network to expand

beyond the sizes we have seen, (2) gene knockdown is not sufficient to cause the effect predicted, or (3) spherule restriction in multifactorial and we only alter a single gene. The first seems unlikely. The *Nrl*-KO retina switches *all* rods to have a cone-like pedicle which takes up more space than our sparse collection of altered spherules. The second and third options are both possible, but we believe that knockdown of multiple independent genes would have a larger effect than a slightly larger reduction in gene expression.

Unlike the spherule width phenotype, we found many genes that reproduced the pedicle OPL localization pattern, and interestingly, these data provide a richer dataset than might be appreciated at first glance because three phenotypes are actually found here: (1) terminals laminating similar to wild type S-cones (the hypothesized effect), (2) spherules found only barely beyond control limits, and (3) axons that bypass the OPL entirely and penetrate into the INL. Are the three phenotypes actually a continuum of a single phenotype? This might be possible. Perhaps higher-level function genes have less of an effect because they are farther removed from the direct affector. Nrl knockdown in our screen for OPL position showed no significantly different effect, and Ncoa2 and Dpf3, two genes we hypothesize are higher-tiered in the new network (Figure 7) also show less of an affect.

One fundamental neurobiology question we have begun to address is how a neuron's morphology and structure affects its function. Above we found multiple loss of function models that show enlarged spherules (Figure 18). We were able to directly assay how increasing the size of the axonal terminal/bouton affected the neurotransmission to the postsynaptic cell. In our tested model, Snta1 knockout, we see both enlarged spherule

size and enhanced neurotransmission in rods without having increased input sensitivity (Figure 18). This is exciting because it provides one of the first models to test the relationship between structure and function directly. Future studies will determine the molecular mechanisms underlying how loss of Snta1 leads to a larger spherule and enhanced scotopic neurotransmission to interneurons. In addition, further testing in other loss of function models with larger spherules, or smaller pedicles, will be required to draw a strong link between the morphological and physiological characteristics of the neuron's terminal. We are excited in how these data open up many avenues of future investigation for both the Snta1 model in photoreceptor synaptic function and for the neurobiology field.

Our dataset provides a solid foundation to begin describing the multigenic program underlying spherule morphogenesis, but its special value lies in the creation of a hypothesis-forming protein network. Within our original, larger network, we defined many connected pathways centering around and traversing through Ncoa2, so we propose a new hypothesis in which a tiered regulatory system (initiating at Nrl, coordinated through Ncoa2, and terminating with multiple affector genes) defines and restricts spherule morphology in developing rod photoreceptors. Ncoa2's method of control over this network still needs to be determined. The steroid receptor protein family, including Ncoa2, are a group of coactivators that in concert with chromatin remodeling proteins (here likely Dpf3 and Smarcd3) permit transcriptional activity (Johnson and O'Malley, 2012). We propose that gene expression controlled through Ncao2-directed transcription will lead to further developments in understanding control of spherule size restriction and terminal position in the OPL.

The larger implication of our work is to utilize these data, especially the protein network, to improve retinal degeneration treatment studies. Retinal reprogramming to re-form neural circuitry following ablation does not completely recapitulate developmental patterns (D'Orazi et al., 2016), so either variations in the intrinsic genetic program and/or the extrinsic cellular environment are responsible for this mismatch of connectivity. Loss of signaling molecules found during development might prevent full integration of new photoreceptors in the adult retina. Perhaps gene expression in transplanted photoreceptors will need to be artificially manipulated to polarize the cells correctly and form native circuitry. Future studies merging iPSC-derived photoreceptor precursors with a gene – therapy-like manipulation of gene expression prior to transplantation would show if our synaptic terminal networks truly mediate proper morphology and connectivity in the retina.

Methods

Animals

The Animal Care and Use Committee of the National Eye Institute (NEI) approved all procedures that involved mice. The following strains were used in the above studies: C57BL/6J, also known as wild type (Jackson Labs 000644), *Nrl*p-EGFP (Jackson Labs 021232), *Nrl*-KO (Jackson Labs 021152), *Nrl*-GFP/*Nrl*-KO, CD-1IGS (Charles River 022), Epb4.1l2-KO ((Sanuki et al., 2015), RIKEN RBRC09370), and Snta1-KO ((Adams et al., 2000), Jackson Labs 012940).

Tissue preparation and immunohistochemistry

After euthanasia, eyes were removed at placed into 4% paraformaldehyde for 10 minutes then retinas were removed and placed back into fixative. For cryosections, retinas were fixed for 1-hour total; for vibratome, retinas were fixed for more than 3 hours.

For cryosections, retinas were frozen into a gel matrix (O.C.T. compound) and were sectioned at a thickness of 14µm onto SuperFrost+ charged slides and allowed to dry overnight to completely adhere to the glass; these were stored at -80°C until use. For immunohistochemistry, slides were blocked in 10% normal donkey serum in 1x PBST (0.3% Triton-X 100) for ≥1 hour. Primary antibodies (below) were incubated in the same solution at 4°C overnight. The following day, slides were washed 3x in 1x PBST for ≥5 minutes then incubated with secondary antibodies in serum solution for 1 hour at room temperature. Slides were washed again 3x in 1x PBST then covered.

For vibratome sections, retinas were mounted into 7% low-melting temperature agar before being sectioned at a thickness of 100µm. Floating sections were stained with DAPI in 1x PBST overnight before being placed onto glass slides and covered.

Antibodies used in this chapter are: DAPI (4',6-Diamidino-2-Phenylindole, Dihydrochloride) to stain DNA, Ribeye for ribbon organelles, Cone arrestin to show full cone structure in all cones, and S-opsin (to label S-cone outer segments).

Gene expression analysis

Gene filtering analysis for rod and cone-like photoreceptors was performed at the gene level using data from a previously published study (Kim et al., 2016b). Absolute fold

changes were used when comparing rod versus cone-like photoreceptors or between developmental stages. For the heat map in Figure 7B, z-scores were used to show dynamic patterns of gene expression independent of absolute expression levels.

In vivo electroporation and AAV injections

We performed electroporations as described previously (Matsuda and Cepko, 2004). Newborn mouse pups (P0-1) were anesthetized via hypothermia (on wet ice) until unresponsive. Eyelids were cleaned with 70% ethanol then dried. A new, sharp 25 gauge needed was used to open the fused junction of the eyelid and expose the underlying eye. A 30.5-gauge needle was used to create a small puncture in the sclera. A 30.5 gauge blunt-ended Hamilton syringe was inserted into the eye to inject 0.2 – 0.3 microliters of DNA plasmid solution into the subretinal space. Immediately following injection, five electrical pulses of 50ms at 80V change with an interval of 950ms between pulses was applied across the entire head using a thumb forceps electrode. The positive electrode is applied on the injected side of the head so that the injected DNA, being negatively charged, is forced into the retina. Only the right eyes were used in this protocol because the electrical charge cannot be applied in opposite directions across the pup's head. Animals were given ketoprofen (2-5mg/kg body weight) subcutaneously before placed on a heated pad to raise body temperature back to physiological levels.

Alteration of cDNA sequences

Full-length cDNAs in the pCMV-Sport6 vector were purchased commercially. Using the New England Biolab's NEBaseChanger, primers to create 5-7 alterations in the shRNA binding sequence were determined. The cDNA was altered using the NEB Q5® Site-Directed Mutagenesis Kit exactly following the instructions provided. Some primer pairs did not produce the appropriate product initially; for these, inclusion of the 5x Q5® Enhancer Buffer was sufficient to obtain the correctly altered products.

Confocal microscopy

Images were collected using the Zeiss 700 and 880 confocal microscopes. A 63x oil-immersion objective, without any digital zoom, was used to image all slides. Images were collected and exported using the Zeiss Zen Black program. For Figures 3 and 4, terminal width and ribbon number images were collected from whole mount retinas using z-axis stacks spaced 0.5μm and flattened into a single image to ensure the largest portion and total ribbon number of the spherules/pedicles was captured. For the OPL position, a single plane image was taken from a retinal section. For the RNAi screen, rescue, and loss-of-function experiments, images were taken from retinal sections. Each spherule (or neighboring clusters) was imaged using enough 0.5 μm z-axis stacks to capture the full width and depth of the spherule.

Quantitative analysis of spherules

All quantitative measurements were performed using the freeware software ImageJ. For Figures 3D and 4 (left), the boarders of each spherule or pedicle was drawn freeform, the area within the boarders were measured, and, assuming circularity, the diameter (width) was calculated. For relative OPL position, the total height of the layer was measured by taking the space between the bottom of the photoreceptor nuclei to the top of the interneuron cell nuclei (Figure 5, "OPL"); synapse position was measured from the top of interneuron nuclei up to the bottom of the ribbon protein staining. A relative location was calculated by taking the synapse position over OPL height. A value of 0 indicates the interneuron nuclei boundary; 1 indicates the photoreceptor nuclei boundary. For the RNAi screen, rescue, and loss-of-function experiments, measurements were collected similarly to above, with a few additions/changes (see Figure 5): terminal width was determined on the retinal sections by taking horizontal measurements of the widest point in the electroporated spherule ("Width"); spherule position was measured from the top of interneuron nuclei to the bottom of the electroporated spherule ("Syn"); and for select terminals, the cell body position ("Cell") and ONL ("ONL") height were measured to determine the relative position of the photoreceptor cell bodies in the ONL.

Electroretinograms

Animals were dark adapted for ≥12 hours. Under red light, animals were given general anesthesia (ketamine, 100mg/kg; xylazine, 10mg/kg) by intraperitoneal injection of 0.1mL/10gram body weight; they were also given a topical anesthetic (0.5% proparacaine

hydrochloride) on each eye. Pupils are dilated using 2.5% phenylephrine and 1% tropicamide. A gold wire is placed non-invasively on the cornea using 2.5% hypomellose ophthalmic demulcent solution and a reference electrode was placed on the tongue. Using the Espion E2 Visual Electrophysiological System, a series of brief photoflashes of light flashes is used to elicit photoreceptor and bipolar retinal cell responses. Scotopic light flashes were recorded first. Six light intensities (log values from 0.0001 to 10 $cd.s.m^{-2}$) were used as stimuli. Immediately following scotopic recordings, six photopic recordings (0.3, 1, 3, 10, 30, and 100 $cd.s.m^{-2}$)

were performed under rod-saturating light. Values were exported to Excel before being graphed in R Studio and statistical analysis performed in Prism (below).

Graphing, statistical analysis, and programs

R Studio and custom ggplot codes were used to generate all graphs. Prism v7 used for all statistical analysis. For figures 4, 9, 10, 11, 14, and 16 we used the Kruskal-Wallis one-way analysis of variance test with Dunn's multiple comparison test. In figure 4, n=30 spherules per location. For figures 10, 1, 14, and 16: we tested $n \geq 1$ animal with ≥ 25 total terminals for each construct (see corresponding tables for exact numbers). For figure 16, we are working to increase our sample size to improve power and reproducibility of our results. In all cases, the following legends are appropriate: n.s. non-significant difference, *p<0.0332, **p<0.0021, ***p<0.0002, ****p<0.0001

Protein interaction networks

Protein-protein interaction data for *Mus musculus* was downloaded from STRING [PMID: 27924014]. Custom scripts were used to filter for high confidence adjacent interactions of our initial set of 720 genes. Clusters and shortest paths in the PPIN were identified using the igraph package (v1.1.2) [Csardi G, Nepusz T: The igraph software package for complex network research, InterJournal, Complex Systems 1695. 2006. http://igraph.org] on R, specifically the random walktrap algorithm was employed to identify communities in the network. All networks were visualized on Cytoscape (v3.6) [PMID: 17947979].

CHAPTER III

CONCLUSIONS AND FUTURE DIRECTIONS

Visual detection of our external environment allows us to navigate the world around us as well as perform many of the tasks that so many of us take for granted. A large proportion of the population sees the loss of vision as the worst possible affliction, equal or worse than that of the other senses or memory or even loss of a limb (Scott et al., 2016). Retinitis pigmentosa (RP), which is defined by the loss of photoreceptors in the retina, is the most common type of RDD, with frequency rates estimated at 1:3,000-7,000 (Ferrari et al., 2011). As mentioned in previous chapters, there are multiple possible treatment strategies that could possibly be employed, including but not limited to: gene therapy, cell therapy, and cellular reprogramming. The use and efficacy of one or more strategy in each patient might be determined based on the timing of disease. If the disease is caught early and a simple genetic variation can be definitively determined to be the causative mutation, gene therapy to correct that singular mutation in existing photoreceptors to prevent disruption of the native system. If the disease has already progressed too far, as would be the case for currently blind RP patients, cell therapy or reprogramming are the only options, though likely both would also require gene therapy if the patient's own cells were to be used. The rapid advancement of the stem cell field in generating retinal cell types, including both rod and cone photoreceptor precursors, is providing a lot of promise that future clinicians might derive iPSCs from a skin biopsy, generate gene therapy-corrected photoreceptor precursors *in vitro*, and reintroduce these cells back into the retina to correct vision. It

seems likely that these steps will likely be possible very soon, and in fact are already in trials to transplant newly derived retinal pigment epithelium (RPE) cells behind the retina for another common RDD (Mandai et al., 2017). Our current hurdle now becomes not derivation or transplantation of photoreceptors but polarization of the cells and integration into the retina circuitry. Early reports were very promising (MacLaren et al., 2006) but were later re-evaluated because material transfer between cells instead of integration was occurring if any photoreceptors remained alive (Singh et al., 2013), though end-stage degeneration integration still seems promising. Current methods to determine integration, protein expression and relative localization, should be more in their analysis. As seen in the first chapter, photoreceptors have highly specific morphologies and connections to interneurons but the molecular factors that determined each of these features in photoreceptors has been lacking. Our current work set out to address this need within the field. We used a semi-directed screening approach to begin identifying the genetic determinants of photoreceptor morphology and positioning for synaptogenesis. While the genes we discovered to play a role in rod spherule morphology likely only scratch the surface of those involved, we also provide a Nrl-centered protein network that could be engaged to create the specific features needed to correctly structure and position axon terminals. Validation and expansion of this network is beyond the scope of our current work, but these at least give us a small view into how we can start adjusting gene expression to manipulate morphology and circuitry within photoreceptors. Below we identify some remaining questions that remain in our field.

Future avenues of investigation

- Structure/function relationship: Does spherule size affect neurotransmission output?
- Control of ribbon number: Like terminal width and OPL position, ribbons are likely genetically controlled. What genes are associated with determining ribbon number?
- Multi-factorial control: Can manipulation of multiple genes (or pathways) have a greater effect on spherule morphology?
- Neural circuitry development: Is neurotransmission from photoreceptors required for synaptogenesis with bipolar and horizontal cells?
- Patient iPSCs: For the genes identified in our screen, are there patients with visual defects in these genes? If yes, how do spherules mature in these human models?

REFERENCES

Abd-El-Barr MM, Pennesi ME, Saszik SM, Barrow AJ, Lem J, Bramblett DE, Paul DL, Frishman LJ, Wu SM (2009) Genetic dissection of rod and cone pathways in the dark-adapted mouse retina. J Neurophysiol 102:1945-1955.

Adams ME, Kramarcy N, Krall SP, Rossi SG, Rotundo RL, Sealock R, Froehner SC (2000) Absence of alpha-syntrophin leads to structurally aberrant neuromuscular synapses deficient in utrophin. J Cell Biol 150:1385-1398.

Alpadi K, Magupalli VG, Kappel S, Koblitz L, Schwarz K, Seigel GM, Sung CH, Schmitz F (2008) RIBEYE recruits Munc119, a mammalian ortholog of the Caenorhabditis elegans protein unc119, to synaptic ribbons of photoreceptor synapses. J Biol Chem 283:26461-26467.

Anastassov IA, Wang W, Dunn FA (2017) Synaptogenesis and synaptic protein localization in the postnatal development of rod bipolar cell dendrites in mouse retina. J Comp Neurol. [Epub ahead of print] https://doi.org/10.1002/cne.24251

Asteriti S, Gargini C, Cangiano L (2014) Mouse rods signal through gap junctions with cones. Elife 3:e01386.

Azevedo FA, Carvalho LR, Grinberg LT, Farfel JM, Ferretti RE, Leite RE, Jacob Filho W, Lent R, Herculano-Houzel S (2009) Equal numbers of neuronal and nonneuronal cells make the human brain an isometrically scaled-up primate brain. J Comp Neurol 513:532-541.

Babai N, Sendelbeck A, Regus-Leidig H, Fuchs M, Mertins J, Reim K, Brose N, Feigenspan A, Brandstatter JH (2016) Functional Roles of Complexin 3 and

Complexin 4 at Mouse Photoreceptor Ribbon Synapses. J Neurosci 36:6651-6667.

Baden T, Euler T, Weckstrom M, Lagnado L (2013) Spikes and ribbon synapses in early vision. Trends Neurosci 36:480-488.

Baek ST, Kerjan G, Bielas SL, Lee JE, Fenstermaker AG, Novarino G, Gleeson JG (2014) Off-target effect of doublecortin family shRNA on neuronal migration associated with endogenous microRNA dysregulation. Neuron 82:1255-1262.

Barber AC, Hippert C, Duran Y, West EL, Bainbridge JW, Warre-Cornish K, Luhmann UF, Lakowski J, Sowden JC, Ali RR, Pearson RA (2013) Repair of the degenerate retina by photoreceptor transplantation. Proc Natl Acad Sci U S A 110:354-359.

Barnes CS, Alexander KR, Fishman GA (2002) A distinctive form of congenital stationary night blindness with cone ON-pathway dysfunction. Ophthalmology 109:575-583.

Baylor DA, Fuortes MG, O'Bryan PM (1971) Receptive fields of cones in the retina of the turtle. J Physiol 214:265-294.

Bech-Hansen NT, Naylor MJ, Maybaum TA, Pearce WG, Koop B, Fishman GA, Mets M, Musarella MA, Boycott KM (1998) Loss-of-function mutations in a calcium-channel alpha1-subunit gene in Xp11.23 cause incomplete X-linked congenital stationary night blindness. Nat Genet 19:264-267.

Berger W, Kloeckener-Gruissem B, Neidhardt J (2010) The molecular basis of human retinal and vitreoretinal diseases. Prog Retin Eye Res 29:335-375.

Blanks JC, Adinolfi AM, Lolley RN (1974) Synaptogenesis in the photoreceptor terminal of the mouse retina. J Comp Neurol 156:81-93.

Bloomfield SA, Volgyi B (2009) The diverse functional roles and regulation of neuronal gap junctions in the retina. Nat Rev Neurosci 10:495-506.

Bolte P, Herrling R, Dorgau B, Schultz K, Feigenspan A, Weiler R, Dedek K, Janssen-Bienhold U (2016) Expression and Localization of Connexins in the Outer Retina of the Mouse. J Mol Neurosci 58:178-192.

Breuninger T, Puller C, Haverkamp S, Euler T (2011) Chromatic bipolar cell pathways in the mouse retina. J Neurosci 31:6504-6517.

Brzezinski JA, Reh TA (2015) Photoreceptor cell fate specification in vertebrates. Development 142:3263-3273.

Cao Y, Sarria I, Fehlhaber KE, Kamasawa N, Orlandi C, James KN, Hazen JL, Gardner MR, Farzan M, Lee A, Baker S, Baldwin K, Sampath AP, Martemyanov KA (2015) Mechanism for Selective Synaptic Wiring of Rod Photoreceptors into the Retinal Circuitry and Its Role in Vision. Neuron 87:1248-1260.

Chen M, Van Hook MJ, Zenisek D, Thoreson WB (2013) Properties of ribbon and non-ribbon release from rod photoreceptors revealed by visualizing individual synaptic vesicles. J Neurosci 33:2071-2086.

Cohen AI (1965) Some electron microscopic observations on inter-receptor contacts in the human and macaque retinae. J Anat 99:595-610.

Cohen E, Sterling P (1990) Convergence and divergence of cones onto bipolar cells in the central area of cat retina. Philos Trans R Soc Lond B Biol Sci 330:323-328.

Congdon N, O'Colmain B, Klaver CC, Klein R, Munoz B, Friedman DS, Kempen J, Taylor HR, Mitchell P, Eye Diseases Prevalence Research G (2004) Causes and prevalence of visual impairment among adults in the United States. Arch Ophthalmol 122:477-485.

Cooper B, Hemmerlein M, Ammermuller J, Imig C, Reim K, Lipstein N, Kalla S, Kawabe H, Brose N, Brandstatter JH, Varoqueaux F (2012) Munc13-independent vesicle priming at mouse photoreceptor ribbon synapses. J Neurosci 32:8040-8052.

Corbo JC, Lawrence KA, Karlstetter M, Myers CA, Abdelaziz M, Dirkes W, Weigelt K, Seifert M, Benes V, Fritsche LG, Weber BH, Langmann T (2010) CRX ChIP-seq reveals the cis-regulatory architecture of mouse photoreceptors. Genome Res 20:1512-1525.

D'Orazi FD, Zhao XF, Wong RO, Yoshimatsu T (2016) Mismatch of Synaptic Patterns between Neurons Produced in Regeneration and during Development of the Vertebrate Retina. Curr Biol 26:2268-2279.

Datta P, Gilliam J, Thoreson WB, Janz R, Heidelberger R (2017) Two Pools of Vesicles Associated with Synaptic Ribbons Are Molecularly Prepared for Release. Biophys J 113:2281-2298.

De Robertis E, Franchi CM (1956) Electron microscope observations on synaptic vesicles in synapses of the retinal rods and cones. J Biophys Biochem Cytol 2:307-318.

Deans MR, Volgyi B, Goodenough DA, Bloomfield SA, Paul DL (2002) Connexin36 is essential for transmission of rod-mediated visual signals in the mammalian retina. Neuron 36:703-712.

Demb JB, Singer JH (2015) Functional Circuitry of the Retina. Annu Rev Vis Sci 1:263-289.

DeVries SH, Qi X, Smith R, Makous W, Sterling P (2002) Electrical coupling between mammalian cones. Curr Biol 12:1900-1907.

Dick O, tom Dieck S, Altrock WD, Ammermuller J, Weiler R, Garner CC, Gundelfinger ED, Brandstatter JH (2003) The presynaptic active zone protein bassoon is essential for photoreceptor ribbon synapse formation in the retina. Neuron 37:775-786.

Dowling JE, Boycott BB (1966) Organization of the primate retina: electron microscopy. Proc R Soc Lond B Biol Sci 166:80-111.

Dunn FA, Wong RO (2012) Diverse strategies engaged in establishing stereotypic wiring patterns among neurons sharing a common input at the visual system's first synapse. J Neurosci 32:10306-10317.

Dunn FA, Della Santina L, Parker ED, Wong RO (2013) Sensory experience shapes the development of the visual system's first synapse. Neuron 80:1159-1166.

Euler T, Haverkamp S, Schubert T, Baden T (2014) Retinal bipolar cells: elementary building blocks of vision. Nat Rev Neurosci 15:507-519.

Fadool JM (2003) Development of a rod photoreceptor mosaic revealed in transgenic zebrafish. Dev Biol 258:277-290.

Feigenspan A, Janssen-Bienhold U, Hormuzdi S, Monyer H, Degen J, Sohl G, Willecke K, Ammermuller J, Weiler R (2004) Expression of connexin36 in cone pedicles and OFF-cone bipolar cells of the mouse retina. J Neurosci 24:3325-3334.

Ferrari S, Di Iorio E, Barbaro V, Ponzin D, Sorrentino FS, Parmeggiani F (2011) Retinitis pigmentosa: genes and disease mechanisms. Curr Genomics 12:238-249.

Frank T, Rutherford MA, Strenzke N, Neef A, Pangrsic T, Khimich D, Fejtova A, Gundelfinger ED, Liberman MC, Harke B, Bryan KE, Lee A, Egner A, Riedel D, Moser T (2010) Bassoon and the synaptic ribbon organize Ca(2)+ channels and vesicles to add release sites and promote refilling. Neuron 68:724-738.

Friedman DS, O'Colmain BJ, Munoz B, Tomany SC, McCarty C, de Jong PT, Nemesure B, Mitchell P, Kempen J, Eye Diseases Prevalence Research G (2004) Prevalence of age-related macular degeneration in the United States. Arch Ophthalmol 122:564-572.

Goede P, Kolb H (1994) Identification of the synaptic pedicles belonging to the different spectral types of photoreceptor in the turtle retina. Vision Res 34:2801-2811.

Graydon CW, Manor U, Kindt KS (2017) In Vivo Ribbon Mobility and Turnover of Ribeye at Zebrafish Hair Cell Synapses. Sci Rep 7:7467.

Graydon CW, Zhang J, Oesch NW, Sousa AA, Leapman RD, Diamond JS (2014) Passive diffusion as a mechanism underlying ribbon synapse vesicle release and resupply. J Neurosci 34:8948-8962.

Gregory-Evans CY, Wallace VA, Gregory-Evans K (2013) Gene networks: dissecting pathways in retinal development and disease. Prog Retin Eye Res 33:40-66.

Grocott T, Tambalo M, Streit A (2012) The peripheral sensory nervous system in the vertebrate head: a gene regulatory perspective. Dev Biol 370:3-23.

Haeseleer F, Imanishi Y, Maeda T, Possin DE, Maeda A, Lee A, Rieke F, Palczewski K (2004) Essential role of Ca2+-binding protein 4, a Cav1.4 channel regulator, in photoreceptor synaptic function. Nat Neurosci 7:1079-1087.

Hagstrom SA, North MA, Nishina PL, Berson EL, Dryja TP (1998) Recessive mutations in the gene encoding the tubby-like protein TULP1 in patients with retinitis pigmentosa. Nat Genet 18:174-176.

Hao H, Kim DS, Klocke B, Johnson KR, Cui K, Gotoh N, Zang C, Gregorski J, Gieser L, Peng W, Fann Y, Seifert M, Zhao K, Swaroop A (2012) Transcriptional regulation of rod photoreceptor homeostasis revealed by in vivo NRL targetome analysis. PLoS Genet 8:e1002649.

Hartong DT, Berson EL, Dryja TP (2006) Retinitis pigmentosa. Lancet 368:1795-1809.

Heidelberger R, Sterling P, Matthews G (2002) Roles of ATP in depletion and replenishment of the releasable pool of synaptic vesicles. J Neurophysiol 88:98-106.

Heidelberger R, Thoreson WB, Witkovsky P (2005) Synaptic transmission at retinal ribbon synapses. Prog Retin Eye Res 24:682-720.

Holt M, Cooke A, Neef A, Lagnado L (2004) High mobility of vesicles supports continuous exocytosis at a ribbon synapse. Curr Biol 14:173-183.

Hoon M, Okawa H, Della Santina L, Wong RO (2014) Functional architecture of the retina: development and disease. Prog Retin Eye Res 42:44-84.

Hornstein EP, Verweij J, Schnapf JL (2004) Electrical coupling between red and green cones in primate retina. Nat Neurosci 7:745-750.

Hornstein EP, Verweij J, Li PH, Schnapf JL (2005) Gap-junctional coupling and absolute sensitivity of photoreceptors in macaque retina. J Neurosci 25:11201-11209.

Hsu A, Smith RG, Buchsbaum G, Sterling P (2000) Cost of cone coupling to trichromacy in primate fovea. J Opt Soc Am A Opt Image Sci Vis 17:635-640.

Johnson AB, O'Malley BW (2012) Steroid receptor coactivators 1, 2, and 3: critical regulators of nuclear receptor activity and steroid receptor modulator (SRM)-based cancer therapy. Mol Cell Endocrinol 348:430-439.

Johnson S, Halford S, Morris AG, Patel RJ, Wilkie SE, Hardcastle AJ, Moore AT, Zhang K, Hunt DM (2003) Genomic organisation and alternative splicing of human RIM1, a gene implicated in autosomal dominant cone-rod dystrophy (CORD7). Genomics 81:304-314.

Jorstad NL, Wilken MS, Grimes WN, Wohl SG, VandenBosch LS, Yoshimatsu T, Wong RO, Rieke F, Reh TA (2017) Stimulation of functional neuronal regeneration from Muller glia in adult mice. Nature 548:103-107.

Kamachi Y, Kondoh H (2013) Sox proteins: regulators of cell fate specification and differentiation. Development 140:4129-4144.

Kelsell RE, Gregory-Evans K, Gregory-Evans CY, Holder GE, Jay MR, Weber BH, Moore AT, Bird AC, Hunt DM (1998) Localization of a gene (CORD7) for a dominant cone-rod dystrophy to chromosome 6q. Am J Hum Genet 63:274-279.

Kim JW, Yang HJ, Oel AP, Brooks MJ, Jia L, Plachetzki DC, Li W, Allison WT, Swaroop A (2016a) Recruitment of Rod Photoreceptors from Short-Wavelength-Sensitive Cones during the Evolution of Nocturnal Vision in Mammals. Dev Cell 37:520-532.

Kim JW, Yang HJ, Brooks MJ, Zelinger L, Karakulah G, Gotoh N, Boleda A, Gieser L, Giuste F, Whitaker DT, Walton A, Villasmil R, Barb JJ, Munson PJ, Kaya KD, Chaitankar V, Cogliati T, Swaroop A (2016b) NRL-Regulated Transcriptome Dynamics of Developing Rod Photoreceptors. Cell Rep 17:2460-2473.

Kolb H (1970) Organization of the outer plexiform layer of the primate retina: electron microscopy of Golgi-impregnated cells. Philos Trans R Soc Lond B Biol Sci 258:261-283.

Kolb H (1977) The organization of the outer plexiform layer in the retina of the cat: electron microscopic observations. J Neurocytol 6:131-153.

Kothmann WW, Li X, Burr GS, O'Brien J (2007) Connexin 35/36 is phosphorylated at regulatory sites in the retina. Vis Neurosci 24:363-375.

Lamb TD, Collin SP, Pugh EN, Jr. (2007) Evolution of the vertebrate eye: opsins, photoreceptors, retina and eye cup. Nat Rev Neurosci 8:960-976.

Lee EJ, Han JW, Kim HJ, Kim IB, Lee MY, Oh SJ, Chung JW, Chun MH (2003) The immunocytochemical localization of connexin 36 at rod and cone gap junctions in the guinea pig retina. Eur J Neurosci 18:2925-2934.

Lee R, Wong TY, Sabanayagam C (2015) Epidemiology of diabetic retinopathy, diabetic macular edema and related vision loss. Eye Vis (Lond) 2:17.

Lee SK, Pfaff SL (2001) Transcriptional networks regulating neuronal identity in the developing spinal cord. Nat Neurosci 4 Suppl:1183-1191.

Li H, Chuang AZ, O'Brien J (2009a) Photoreceptor coupling is controlled by connexin 35 phosphorylation in zebrafish retina. J Neurosci 29:15178-15186.

Li H, Zhang Z, Blackburn MR, Wang SW, Ribelayga CP, O'Brien J (2013) Adenosine and dopamine receptors coregulate photoreceptor coupling via gap junction phosphorylation in mouse retina. J Neurosci 33:3135-3150.

Li Z, Sergouniotis PI, Michaelides M, Mackay DS, Wright GA, Devery S, Moore AT, Holder GE, Robson AG, Webster AR (2009b) Recessive mutations of the gene TRPM1 abrogate ON bipolar cell function and cause complete congenital stationary night blindness in humans. Am J Hum Genet 85:711-719.

Lv C, Stewart WJ, Akanyeti O, Frederick C, Zhu J, Santos-Sacchi J, Sheets L, Liao JC, Zenisek D (2016) Synaptic Ribbons Require Ribeye for Electron Density, Proper Synaptic Localization, and Recruitment of Calcium Channels. Cell Rep 15:2784-2795.

MacLaren RE, Pearson RA, MacNeil A, Douglas RH, Salt TE, Akimoto M, Swaroop A, Sowden JC, Ali RR (2006) Retinal repair by transplantation of photoreceptor precursors. Nature 444:203-207.

Magupalli VG, Schwarz K, Alpadi K, Natarajan S, Seigel GM, Schmitz F (2008) Multiple RIBEYE-RIBEYE interactions create a dynamic scaffold for the formation of synaptic ribbons. J Neurosci 28:7954-7967.

Malihi M, Moura Filho ER, Hodge DO, Sit AJ (2014) Long-term trends in glaucoma-related blindness in Olmsted County, Minnesota. Ophthalmology 121:134-141.

Mandai M et al. (2017) Autologous Induced Stem-Cell-Derived Retinal Cells for Macular Degeneration. N Engl J Med 376:1038-1046.

Masland RH (2001a) The fundamental plan of the retina. Nat Neurosci 4:877-886.

Masland RH (2001b) Neuronal diversity in the retina. Curr Opin Neurobiol 11:431-436.

Masland RH (2012) The neuronal organization of the retina. Neuron 76:266-280.

Matsuda T, Cepko CL (2004) Electroporation and RNA interference in the rodent retina in vivo and in vitro. Proc Natl Acad Sci U S A 101:16-22.

Matthews G, Fuchs P (2010) The diverse roles of ribbon synapses in sensory neurotransmission. Nat Rev Neurosci 11:812-822.

Maxeiner S, Luo F, Tan A, Schmitz F, Sudhof TC (2016) How to make a synaptic ribbon: RIBEYE deletion abolishes ribbons in retinal synapses and disrupts neurotransmitter release. EMBO J 35:1098-1114.

Mears AJ, Kondo M, Swain PK, Takada Y, Bush RA, Saunders TL, Sieving PA, Swaroop A (2001) Nrl is required for rod photoreceptor development. Nat Genet 29:447-452.

Mehta B, Snellman J, Chen S, Li W, Zenisek D (2013) Synaptic ribbons influence the size and frequency of miniature-like evoked postsynaptic currents. Neuron 77:516-527.

Mitton KP, Swain PK, Chen S, Xu S, Zack DJ, Swaroop A (2000) The leucine zipper of NRL interacts with the CRX homeodomain. A possible mechanism of transcriptional synergy in rhodopsin regulation. J Biol Chem 275:29794-29799.

Morgan JL, Dhingra A, Vardi N, Wong RO (2006) Axons and dendrites originate from neuroepithelial-like processes of retinal bipolar cells. Nat Neurosci 9:85-92.

Muresan V, Lyass A, Schnapp BJ (1999) The kinesin motor KIF3A is a component of the presynaptic ribbon in vertebrate photoreceptors. J Neurosci 19:1027-1037.

Noel NCL, Allison WT (2017) Connectivity of cone photoreceptor telodendria in the zebrafish retina. J Comp Neurol.

O'Brien J, al-Ubaidi MR, Ripps H (1996) Connexin 35: a gap-junctional protein expressed preferentially in the skate retina. Mol Biol Cell 7:233-243.

O'Brien JJ, Chen X, Macleish PR, O'Brien J, Massey SC (2012) Photoreceptor coupling mediated by connexin36 in the primate retina. J Neurosci 32:4675-4687.

Oh EC, Khan N, Novelli E, Khanna H, Strettoi E, Swaroop A (2007) Transformation of cone precursors to functional rod photoreceptors by bZIP transcription factor NRL. Proc Natl Acad Sci U S A 104:1679-1684.

Oh EC, Cheng H, Hao H, Jia L, Khan NW, Swaroop A (2008) Rod differentiation factor NRL activates the expression of nuclear receptor NR2E3 to suppress the development of cone photoreceptors. Brain Res 1236:16-29.

Ohtsuka T, Kawamata K (1990) Telodendrial contact of HRP-filled photoreceptors in the turtle retina: pathways of photoreceptor coupling. J Comp Neurol 292:599-613.

Olney JW (1968) An electron microscopic study of synapse formation, receptor outer segment development, and other aspects of developing mouse retina. Invest Ophthalmol 7:250-268.

Omori Y, Araki F, Chaya T, Kajimura N, Irie S, Terada K, Muranishi Y, Tsujii T, Ueno S, Koyasu T, Tamaki Y, Kondo M, Amano S, Furukawa T (2012) Presynaptic dystroglycan-pikachurin complex regulates the proper synaptic connection between retinal photoreceptor and bipolar cells. J Neurosci 32:6126-6137.

Ou J, Vijayasarathy C, Ziccardi L, Chen S, Zeng Y, Marangoni D, Pope JG, Bush RA, Wu Z, Li W, Sieving PA (2015) Synaptic pathology and therapeutic repair in adult retinoschisis mouse by AAV-RS1 transfer. J Clin Invest 125:2891-2903.

Ouyang X, Winbow VM, Patel LS, Burr GS, Mitchell CK, O'Brien J (2005) Protein kinase A mediates regulation of gap junctions containing connexin35 through a complex pathway. Brain Res Mol Brain Res 135:1-11.

Pakkenberg B, Pelvig D, Marner L, Bundgaard MJ, Gundersen HJ, Nyengaard JR, Regeur L (2003) Aging and the human neocortex. Exp Gerontol 38:95-99.

Pearson RA, Gonzalez-Cordero A, West EL, Ribeiro JR, Aghaizu N, Goh D, Sampson RD, Georgiadis A, Waldron PV, Duran Y, Naeem A, Kloc M, Cristante E, Kruczek K, Warre-Cornish K, Sowden JC, Smith AJ, Ali RR (2016) Donor and host photoreceptors engage in material transfer following transplantation of post-mitotic photoreceptor precursors. Nat Commun 7:13029.

Peichl L, Gonzalez-Soriano J (1994) Morphological types of horizontal cell in rodent retinae: a comparison of rat, mouse, gerbil, and guinea pig. Vis Neurosci 11:501-517.

Perge JA, Niven JE, Mugnaini E, Balasubramanian V, Sterling P (2012) Why do axons differ in caliber? J Neurosci 32:626-638.

Prokop A, Meinertzhagen IA (2006) Development and structure of synaptic contacts in Drosophila. Semin Cell Dev Biol 17:20-30.

Publio R, Oliveira RF, Roque AC (2009) A computational study on the role of gap junctions and rod Ih conductance in the enhancement of the dynamic range of the retina. PLoS One 4:e6970.

Rabl K, Cadetti L, Thoreson WB (2005) Kinetics of exocytosis is faster in cones than in rods. J Neurosci 25:4633-4640.

Rao-Mirotznik R, Harkins AB, Buchsbaum G, Sterling P (1995) Mammalian rod terminal: architecture of a binary synapse. Neuron 14:561-569.

Ratnapriya R, Swaroop A (2013) Genetic architecture of retinal and macular degenerative diseases: the promise and challenges of next-generation sequencing. Genome Med 5:84.

Raviola E, Gilula NB (1973) Gap junctions between photoreceptor cells in the vertebrate retina. Proc Natl Acad Sci U S A 70:1677-1681.

Raviola E, Gilula NB (1975) Intramembrane organization of specialized contacts in the outer plexiform layer of the retina. A freeze-fracture study in monkeys and rabbits. J Cell Biol 65:192-222.

Regus-Leidig H, tom Dieck S, Brandstatter JH (2010) Absence of functional active zone protein Bassoon affects assembly and transport of ribbon precursors during early steps of photoreceptor synaptogenesis. Eur J Cell Biol 89:468-475.

Regus-Leidig H, Tom Dieck S, Specht D, Meyer L, Brandstatter JH (2009) Early steps in the assembly of photoreceptor ribbon synapses in the mouse retina: the involvement of precursor spheres. J Comp Neurol 512:814-824.

Regus-Leidig H, Fuchs M, Lohner M, Leist SR, Leal-Ortiz S, Chiodo VA, Hauswirth WW, Garner CC, Brandstatter JH (2014) In vivo knockdown of Piccolino disrupts presynaptic ribbon morphology in mouse photoreceptor synapses. Front Cell Neurosci 8:259.

Regus-Leidig H, Ott C, Lohner M, Atorf J, Fuchs M, Sedmak T, Kremers J, Fejtova A, Gundelfinger ED, Brandstatter JH (2013) Identification and immunocytochemical characterization of Piccolino, a novel Piccolo splice variant selectively expressed at sensory ribbon synapses of the eye and ear. PLoS One 8:e70373.

Rehemtulla A, Warwar R, Kumar R, Ji X, Zack DJ, Swaroop A (1996) The basic motif-leucine zipper transcription factor Nrl can positively regulate rhodopsin gene expression. Proc Natl Acad Sci U S A 93:191-195.

Ribelayga C, Cao Y, Mangel SC (2008) The circadian clock in the retina controls rod-cone coupling. Neuron 59:790-801.

Rich KA, Zhan Y, Blanks JC (1997) Migration and synaptogenesis of cone photoreceptors in the developing mouse retina. J Comp Neurol 388:47-63.

Rizzoli SO, Betz WJ (2005) Synaptic vesicle pools. Nat Rev Neurosci 6:57-69.

Sanes JR, Yamagata M (2009) Many paths to synaptic specificity. Annu Rev Cell Dev Biol 25:161-195.

Sanes JR, Zipursky SL (2010) Design principles of insect and vertebrate visual systems. Neuron 66:15-36.

Sanuki R, Watanabe S, Sugita Y, Irie S, Kozuka T, Shimada M, Ueno S, Usukura J, Furukawa T (2015) Protein-4.1G-Mediated Membrane Trafficking Is Essential for Correct Rod Synaptic Location in the Retina and for Normal Visual Function. Cell Rep.

Sato S, Omori Y, Katoh K, Kondo M, Kanagawa M, Miyata K, Funabiki K, Koyasu T, Kajimura N, Miyoshi T, Sawai H, Kobayashi K, Tani A, Toda T, Usukura J, Tano Y, Fujikado T, Furukawa T (2008) Pikachurin, a dystroglycan ligand, is essential for photoreceptor ribbon synapse formation. Nat Neurosci 11:923-931.

Schmitz F, Konigstorfer A, Sudhof TC (2000) RIBEYE, a component of synaptic ribbons: a protein's journey through evolution provides insight into synaptic ribbon function. Neuron 28:857-872.

Scott AW, Bressler NM, Ffolkes S, Wittenborn JS, Jorkasky J (2016) Public Attitudes About Eye and Vision Health. JAMA Ophthalmol 134:1111-1118.

Singh MS, Charbel Issa P, Butler R, Martin C, Lipinski DM, Sekaran S, Barnard AR, MacLaren RE (2013) Reversal of end-stage retinal degeneration and restoration of visual function by photoreceptor transplantation. Proc Natl Acad Sci U S A 110:1101-1106.

Siskova Z, Justus D, Kaneko H, Friedrichs D, Henneberg N, Beutel T, Pitsch J, Schoch S, Becker A, von der Kammer H, Remy S (2014) Dendritic structural degeneration is functionally linked to cellular hyperexcitability in a mouse model of Alzheimer's disease. Neuron 84:1023-1033.

Snellman J, Mehta B, Babai N, Bartoletti TM, Akmentin W, Francis A, Matthews G, Thoreson W, Zenisek D (2011) Acute destruction of the synaptic ribbon reveals a role for the ribbon in vesicle priming. Nat Neurosci 14:1135-1141.

Sohl G, Degen J, Teubner B, Willecke K (1998) The murine gap junction gene connexin36 is highly expressed in mouse retina and regulated during brain development. FEBS Lett 428:27-31.

Soto F, Watkins KL, Johnson RE, Schottler F, Kerschensteiner D (2013) NGL-2 regulates pathway-specific neurite growth and lamination, synapse formation, and signal transmission in the retina. J Neurosci 33:11949-11959.

Stone EM (2009) Progress toward effective treatments for human photoreceptor degenerations. Curr Opin Genet Dev 19:283-289.

Strettoi E, Dacheux RF, Raviola E (1990) Synaptic connections of rod bipolar cells in the inner plexiform layer of the rabbit retina. J Comp Neurol 295:449-466.

Strettoi E, Raviola E, Dacheux RF (1992) Synaptic connections of the narrow-field, bistratified rod amacrine cell (AII) in the rabbit retina. J Comp Neurol 325:152-168.

Strettoi E, Mears AJ, Swaroop A (2004) Recruitment of the rod pathway by cones in the absence of rods. J Neurosci 24:7576-7582.

Sudhof TC (2012) The presynaptic active zone. Neuron 75:11-25.

Swaroop A, Kim D, Forrest D (2010) Transcriptional regulation of photoreceptor development and homeostasis in the mammalian retina. Nat Rev Neurosci 11:563-576.

Syed MH, Mark B, Doe CQ (2017) Playing Well with Others: Extrinsic Cues Regulate Neural Progenitor Temporal Identity to Generate Neuronal Diversity. Trends Genet 33:933-942.

Szklarczyk D, Morris JH, Cook H, Kuhn M, Wyder S, Simonovic M, Santos A, Doncheva NT, Roth A, Bork P, Jensen LJ, von Mering C (2017) The STRING database in 2017: quality-controlled protein-protein association networks, made broadly accessible. Nucleic Acids Res 45:D362-D368.

Tarboush R, Chapman GB, Connaughton VP (2012) Ultrastructure of the distal retina of the adult zebrafish, Danio rerio. Tissue Cell 44:264-279.

tom Dieck S, Altrock WD, Kessels MM, Qualmann B, Regus H, Brauner D, Fejtova A, Bracko O, Gundelfinger ED, Brandstatter JH (2005) Molecular dissection of the photoreceptor ribbon synapse: physical interaction of Bassoon and RIBEYE is essential for the assembly of the ribbon complex. J Cell Biol 168:825-836.

tom Dieck S, Specht D, Strenzke N, Hida Y, Krishnamoorthy V, Schmidt KF, Inoue E, Ishizaki H, Tanaka-Okamoto M, Miyoshi J, Hagiwara A, Brandstatter JH, Lowel S, Gollisch T, Ohtsuka T, Moser T (2012) Deletion of the presynaptic scaffold CAST reduces active zone size in rod photoreceptors and impairs visual processing. J Neurosci 32:12192-12203.

Tsukamoto Y, Omi N (2013) Functional allocation of synaptic contacts in microcircuits from rods via rod bipolar to AII amacrine cells in the mouse retina. J Comp Neurol 521:3541-3555.

Tsukamoto Y, Morigiwa K, Ueda M, Sterling P (2001) Microcircuits for night vision in mouse retina. J Neurosci 21:8616-8623.

Vaithianathan T, Henry D, Akmentin W, Matthews G (2015) Functional roles of complexin in neurotransmitter release at ribbon synapses of mouse retinal bipolar neurons. J Neurosci 35:4065-4070.

van Genderen MM, Bijveld MM, Claassen YB, Florijn RJ, Pearring JN, Meire FM, McCall MA, Riemslag FC, Gregg RG, Bergen AA, Kamermans M (2009) Mutations in TRPM1 are a common cause of complete congenital stationary night blindness. Am J Hum Genet 85:730-736.

van Rossum MC, Smith RG (1998) Noise removal at the rod synapse of mammalian retina. Vis Neurosci 15:809-821.

van Spronsen M, Hoogenraad CC (2010) Synapse pathology in psychiatric and neurologic disease. Curr Neurol Neurosci Rep 10:207-214.

Veleri S, Lazar CH, Chang B, Sieving PA, Banin E, Swaroop A (2015) Biology and therapy of inherited retinal degenerative disease: insights from mouse models. Dis Model Mech 8:109-129.

Volgyi B, Deans MR, Paul DL, Bloomfield SA (2004) Convergence and segregation of the multiple rod pathways in mammalian retina. J Neurosci 24:11182-11192.

von Gersdorff H, Vardi E, Matthews G, Sterling P (1996) Evidence that vesicles on the synaptic ribbon of retinal bipolar neurons can be rapidly released. Neuron 16:1221-1227.

Wan J, Goldman D (2016) Retina regeneration in zebrafish. Curr Opin Genet Dev 40:41-47.

Wang Y, Okamoto M, Schmitz F, Hofmann K, Sudhof TC (1997) Rim is a putative Rab3 effector in regulating synaptic-vesicle fusion. Nature 388:593-598.

Wassle H (2004) Parallel processing in the mammalian retina. Nat Rev Neurosci 5:747-757.

Wijetunge LS, Angibaud J, Frick A, Kind PC, Nagerl UV (2014) Stimulated emission depletion (STED) microscopy reveals nanoscale defects in the developmental trajectory of dendritic spine morphogenesis in a mouse model of fragile X syndrome. J Neurosci 34:6405-6412.

Wong RO, Ghosh A (2002) Activity-dependent regulation of dendritic growth and patterning. Nat Rev Neurosci 3:803-812.

Wycisk KA, Zeitz C, Feil S, Wittmer M, Forster U, Neidhardt J, Wissinger B, Zrenner E, Wilke R, Kohl S, Berger W (2006) Mutation in the auxiliary calcium-channel subunit CACNA2D4 causes autosomal recessive cone dystrophy. Am J Hum Genet 79:973-977.

Yadav SP, Hao H, Yang HJ, Kautzmann MA, Brooks M, Nellissery J, Klocke B, Seifert M, Swaroop A (2014) The transcription-splicing protein NonO/p54nrb and three NonO-interacting proteins bind to distal enhancer region and augment rhodopsin expression. Hum Mol Genet 23:2132-2144.

Yoshimatsu T, D'Orazi FD, Gamlin CR, Suzuki SC, Suli A, Kimelman D, Raible DW, Wong RO (2016) Presynaptic partner selection during retinal circuit reassembly varies with timing of neuronal regeneration in vivo. Nat Commun 7:10590.

Zarbin M (2016) Cell-Based Therapy for Degenerative Retinal Disease. Trends Mol Med 22:115-134.

Zeitz C, Kloeckener-Gruissem B, Forster U, Kohl S, Magyar I, Wissinger B, Matyas G, Borruat FX, Schorderet DF, Zrenner E, Munier FL, Berger W (2006) Mutations in CABP4, the gene encoding the Ca2+-binding protein 4, cause autosomal recessive night blindness. Am J Hum Genet 79:657-667.

Zeitz C et al. (2013) Whole-exome sequencing identifies LRIT3 mutations as a cause of autosomal-recessive complete congenital stationary night blindness. Am J Hum Genet 92:67-75.

Zhang J, Wu SM (2004) Connexin35/36 gap junction proteins are expressed in photoreceptors of the tiger salamander retina. J Comp Neurol 470:1-12.

Zhang Z, Li H, Liu X, O'Brien J, Ribelayga CP (2015) Circadian clock control of connexin36 phosphorylation in retinal photoreceptors of the CBA/CaJ mouse strain. Vis Neurosci 32:E009.